

# **Model Based Signal Processing for GPR Data Inversion**

by

**Visweswaran Srinivasamurthy**

B.E., Electrical and Electronics Engineering,

University of Madras, 2001

Submitted to the Department of Electrical Engineering and Computer Science and the faculty of the Graduate School of the University of Kansas in partial fulfillment of the requirements for the degree of Master of Science.

---

**Chair: Dr. Sivaprasad Gogineni**

---

**Co-Chair: Dr. Muhammad Dawood**

---

**Dr. Pannirselvam Kanagaratnam**

**Date of Thesis Defense: April 13<sup>th</sup>, 2005**

*At the Divine Lotus Feet of*  
*Bhagawan Sri Sathya Sai Baba*

## ACKNOWLEDGMENTS

I would like to take this opportunity to thank my research advisor Dr. Muhammad Dawood for giving me an opportunity to work on this project and for guiding me throughout this work. In addition to gaining technical knowledge, I learnt from him the importance of hard work, perseverance and a professional approach to life.

I am extremely grateful to Dr. Sivaprasad Gogineni for his guidance and suggestions in this research and also for introducing me to several concepts in the field of radars. I would like to thank Dr. Pannirselvam Kanagaratnam for his immense help in the testing of the algorithm on actual radar data and for helping me complete this work. I would also like to thank him for accepting to serve on my committee.

I would like to acknowledge the technical help received from Vijay Ramasami, Sudarsan Krishnan, Bharath Parthasarathy, John Paden and Bhaskar Natarajakumar during various stages of my research. I would also like to thank Dr. Umberto Spagnolini for clarifying my doubts in implementing the Gauss-Newton Algorithm. It is my duty to thank several of my friends for their inspiring words and support during difficult times.

This work would not have been possible, if not for the love, encouragement and support of my parents and my sister and for the sacrifices that they had to make so that I could earn a Master's degree. I am also deeply indebted to my teachers at Sindhi Model School for laying the foundation for what I am today. I thank my friends in Lawrence for making my stay here a memorable one.

Words cannot describe all that I owe to my beloved *Swami* for his love, guidance and grace. This thesis is an offering at His lotus feet.

## TABLE OF CONTENTS

Abstract .....	x
Chapter 1 Introduction.....	1
1.1 Motivation.....	1
1.2 Radars in Remote Sensing .....	1
1.3 The Model Based Approach .....	4
1.4 Organization.....	6
Chapter 2 Forward Modeling of radar return .....	7
2.1 Plane wave propagation in Multi-layered Media.....	8
2.1.1 Permittivity.....	8
2.2 Wave Propagation Phenomena .....	10
2.2.1 Reflection & Transmission.....	10
2.2.2 Attenuation.....	11
2.3 Modeling Target Response .....	13
2.4 Three Dimensional FDTD modeling .....	16
2.5 Summary .....	16
Chapter 3 The Inverse Problem .....	17
3.1 Parameter Estimation.....	17
3.2 Inversion by Layer Stripping .....	19
3.3 Model Based Estimators .....	22
3.3.1 MMSE Minimization Algorithms.....	23
3.3.1.1 Gauss Newton Method.....	25
3.3.1.2 Kalman Filter Method.....	29
3.3.2 Spectral Estimation Techniques.....	31
3.3.2.1 The MUSIC Algorithm.....	34
3.4 Summary .....	40

Chapter 4 Simulations.....	41
4.1 FMCW Radar Modeling .....	41
4.2 Inversion by Layer – Stripping .....	47
4.2.1 The Problem of sidelobes:.....	51
4.3 Inversion using Gauss-Newton Method.....	53
4.3.1 Example of Parameterization:.....	54
4.3.2 Implementation of the Gauss – Newton Algorithm.....	56
4.4 Inversion using MUSIC .....	62
4.5 Summary .....	69
 Chapter 5 Inversion on actual data.....	 70
5.1 Experiments in Antarctica.....	70
5.1.1 Modeling the complex dielectric constant of snow cover on sea-ice.....	73
5.2 Tests at the Sandbox lab at RSL .....	82
5.3 Experiments in Greenland.....	89
Summary .....	98
 Chapter 6 GUI for the Inversion algorithm.....	 99
 Chapter 7 Summary and Future Work.....	 103
7.1 Summary .....	103
7.2 Future Work.....	104
 References: .....	 105

## LIST OF FIGURES

Figure 1-1 EM phenomenon for a Multilayered target case; A typical permittivity profile.....	3
Figure 1-2 The Model Based Approach for data inversion .....	5
Figure 2-1 Multi-layered target with different dielectric boundaries .....	8
Figure 2-2 Block diagram of the forward modeling problem.....	14
Figure 2-3 Simulation Flowchart .....	15
Figure 3-1 The Least Squares Approach .....	24
Figure 3-2 The concept of Local and Global minimum .....	28
Figure 3-3 FFT Vs Spectral Estimation Algorithm for enhancement of Profile .....	38
Figure 4-1 FMCW - Chirp Waveform.....	41
Figure 4-2 Simplified Model of an FMCW Radar.....	43
Figure 4-3 A Multilayered Profile .....	45
Figure 4-4 Range Profile obtained by taking IFFT.....	46
Figure 4-5 Range Profile obtained using FFT .....	48
Figure 4-6 Actual Vs Reconstructed Permittivity Profile.....	49
Figure 4-7 Range Profile of table 4.3 with thresholds marked .....	50
Figure 4-8 Range profile of table 4-4 .....	52
Figure 4-9 Illustration of parameterization and discretization of depth .....	54
Figure 4-10 Flow chart of the Gauss Newton MMSE estimation algorithm.....	55
Figure 4-11 MMSE Vs No. of iterations for Global Minimum convergence.....	58
Figure 4-12 MMSE Vs No. of iterations for Local Minimum convergence .....	58
Figure 4-13 MMSE Vs No. of iterations for No convergence.....	59
Figure 4-14 Reconstructed Vs Actual Profile of table 4-2 using Gauss Newton Algorithm.....	60
Figure 4-15 Reconstructed Vs actual profile showing local minimum convergence for profile of table 4-2 .....	60
Figure 4-16 Reconstructed Vs actual profile for table 4-6 with SNR of 10 dB.....	61
Figure 4-17 Range profiles obtained using FFT and MUSIC for profile of table 4-2	63

Figure 4-18 Reconstructed Vs assumed profile of table 4-2 using MUSIC algorithm .....	64
Figure 4-19 Range Profiles obtained using FFT and MUSIC for profile of table 4-965	
Figure 4-20 Reconstructed Vs actual permittivity profile of table 4-9.....	65
Figure 4-21 Range Profiles using FFT and MUSIC of table 4-10.....	66
Figure 4-22 Reconstructed Vs assumed profile of table 4-10.....	67
Figure 4-23 Range profile (using MUSIC) depicting enhancement of weaker reflections.....	68
Figure 4-24 Reconstructed profile obtained after including false alarms in the beat frequency vector.....	68
Figure 5-1 Model of the Snow radar used in Antarctica.....	71
Figure 5-2 Permittivity profile of table 5-3.....	75
Figure 5-3 A-scope of radar measurements.....	76
Figure 5-4 Range Profile plot of A-scope 20.....	76
Figure 5-5 Range Profile after calibration and filtering.....	78
Figure 5-6 Range Profiles obtained using FFT and MUSIC.....	78
Figure 5-7 Reconstructed Vs modeled profile for Pit 1.....	79
Figure 5-8 Range Profiles obtained using FFT and MUSIC for Pit 2.....	80
Figure 5-9 Reconstructed Vs modeled profile for Pit 2.....	81
Figure 5-10 Range Profiles obtained using FFT and MUSIC for Pit 3.....	81
Figure 5-11 Reconstructed Vs modeled profile for Pit 3.....	82
Figure 5-12 Multilayered Target stack to test inversion algorithm.....	84
Figure 5-13 Average of 50 sky shot measurements.....	85
Figure 5-14 Measured return from Aluminium plate.....	85
Figure 5-15 Plate return after sky shot removal.....	86
Figure 5-16 Measured return from multilayered stack.....	86
Figure 5-17 Stack return after sky shot removal.....	87
Figure 5-18 Stack return after calibration and filtering.....	87
Figure 5-19 Range Profiles obtained using FFT and MUSIC for multilayered stack	88

Figure 5-20 Reconstructed Vs actual Permittivity profile of multilayered stack .....	89
Figure 5-21 Relative locations of measurement grid and cores.....	91
Figure 5-22 Experimental set up of the plane wave test.....	91
Figure 5-23 Echogram of radar measurements along the KU radar grid.....	92
Figure 5-24 Radar measurement at record 0 (including the impedance mismatch at the origin).....	93
Figure 5-25 Sky shot measurements .....	93
Figure 5-26 Radar measurement at record 0 (after subtracting the sky shot return) .	94
Figure 5-27 Permittivity profile of Pit 2 modeled using the dry snow model .....	95
Figure 5-28 Simulated radar return of Pit 2 using ADS .....	96
Figure 5-29 Actual radar return at record 0 .....	96
Figure 5-30 Range Profiles of simulated data obtained using FFT and MUSIC.....	97
Figure 5-31 Reconstructed permittivity profile Vs actual (modeled) profile .....	98
Figure 6-1 Snapshot of the GUI for Data Inversion .....	100

## LIST OF TABLES

Table 4-1 Radar parameters and geophysical parameters for FMCW radar modeling .....	46
Table 4-2 Radar and geophysical parameters to illustrate layer stripping.....	47
Table 4-3 Profile chosen to illustrate the problem of false alarms and missed peaks .....	49
Table 4-4 Profile chosen to illustrate the problem of sidelobes.....	51
Table 4-5 Geo-profile to illustrate the discretization problem.....	62
Table 4-6 Geo-profile to test MUSIC with random depth profiles.....	64
Table 4-7 Geo-profile to test MUSIC with the problem of sidelobes.....	66
Table 5-1 Parameters of UWB FMCW radar used in Antarctica .....	71
Table 5-2 Snow pit measurements .....	72
Table 5-3 Modeled Permittivity Profile .....	75
Table 5-4 Comparison of estimated beat frequencies of core with those of FFT and MUSIC .....	79
Table 5-5 Network Analyzer Parameters for Sandbox experiment .....	83
Table 5-6 Network Analyzer Parameters for Plane Wave measurements in Greenland .....	90

## Abstract

The use of Ground-penetrating Radar (GPR) for geological exploration, among others, is gaining widespread acceptance. The estimation of electrical parameters (permittivity) from data collected using a Ground Penetrating Radar (GPR), also called *Electromagnetic Inversion (EM) Inversion*, is of immense importance for applications such as sub-surface characterization. Typically, inversion techniques attempt to reconstruct the permittivity profile of the target by comparing the measured target signatures with a model that closely follows the underlying physical phenomenon. This involves a mapping from the 3-dimensional domain to a one-dimensional domain.

However, this is a complicated problem in that the relationship between the dependent parameters and the observed radar data is not a linear one. Also, GPR data are corrupted with noise, scattering components and losses due to the random nature of the underlying subsurface and due to the attenuation of high frequency components through subsurface layers. Therefore, conventional windowing and Fourier Transform techniques are not adequate for the purposes of enhancing the weaker signals embedded in the sidelobes of strong reflections from surface or subsurface layers; and characterizing the surface and sub-surface features, specifically, to estimate the underlying permittivity profile.

Thus, it is necessary to develop a signal processing approach that should minimize the range sidelobes for enhancement of weaker sub-surface features and then estimate the unknown permittivity.

The main focus of this thesis is to develop an inversion technique that can estimate the underlying permittivity, given the GPR data from a multi-layered structure. Conventional methods such as the Fourier transform and MMSE Minimization seem to offer a solution, but suffer from a few limitations. Spectral Estimation techniques were studied and successfully implemented. The performance of all these approaches in simulations and on actual data from field experiments are presented in this thesis. Finally, a GUI for the inversion algorithm is also developed.

# Chapter 1

## Introduction

---

### 1.1 Motivation

NASA has structured the Mars Exploration Program (MEP) [1] for a series of highly ambitious missions to Mars over the next decade. The MEP plans to send several landers/orbiters to Mars to achieve some of the following objectives:

1. To increase the understanding of the availability and amount of water on Mars.
2. To identify the composition of rocks and soils within the Martian surface.
3. To determine the nature of geological processes from surface morphology.
4. To improve understanding of the Mars climate by analysis of *in-situ* materials.

In order to achieve these objectives, we need intelligent remote sensing techniques. In this regard, NASA designed the Mars Instrument Development Project (MIDP) to develop instruments that can be deployed on the Martian surface to gather geological data.

### 1.2 Radars in Remote Sensing

The use of radars in remote sensing of the environment is well known [2]. The primary purpose of radars was to detect the presence of targets. However, with advancement in technology, radars are now being used to characterize the targets

based on their constituents. This is popularly known as the *EM (Electro-Magnetic) Inversion Problem* in Radar - where the goal is to estimate the composition of materials using data collected by a radar. A Ground Penetrating Radar (GPR) uses high frequency electromagnetic waves (typically from 10 MHz to 1,000 MHz) to extract information about targets.

In the field of geology, we come across a fundamental term called stratigraphy, which is defined as the physical distribution of rocks and soils beneath the target surface under observation. From a radar point of view, stratigraphy refers to the distribution of the electrical properties (permittivity and permeability) of materials.

The EM wave radiated from a transmitter antenna travels through different media (at a velocity governed by the electrical properties of the material) and if it encounters a boundary with differing electrical properties, a part of the wave energy is reflected or scattered back to the surface, while part of the energy continues to travel downward. The amplitude of the reflected signal depends on the dielectric contrast between successive media. The radar receiver collects the composite return signal consisting of several returns from various layers of different dielectric constants.

NASA, in association with the Italian Space Agency has developed MARSIS (Mars Advanced Radar for Subsurface and Ionosphere Sounding) to be tested in the Martian surface [3]. This instrument will perform sub-surface sounding of the Martian crust. The collected data will then be processed to characterize subsurface

features. More specifically, scientists are interested to know if water exists on Mars. This forms a major motivating factor for this thesis. Here, we address the problem of estimating the permittivity (dielectric constant) profile of any multi-layered media using GPR recorded data. This necessitates the development of robust signal processing schemes that can estimate the unknown electrical parameters from a composite signal seen by the radar. From a mathematical point of view, this problem is called *Parameter Estimation*. Figure 1-1 illustrates the problem statement pictorially.

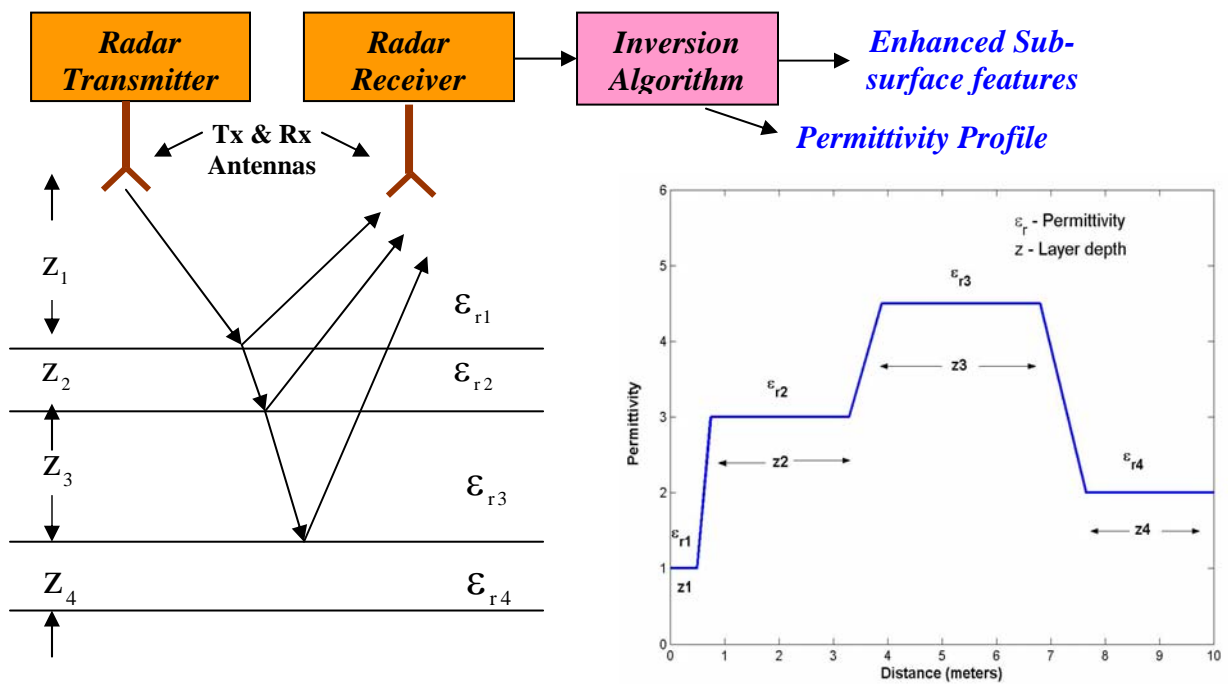


Figure 1-1 EM phenomenon for a Multilayered target case; A typical permittivity profile

There are many problems in estimating the underlying parameters from the radar data. If the radar measures only the reflections from layers with contrast in permittivity, then it is easy to estimate the unknown parameters. However there are

several other factors like scattering, attenuation and additive noise that corrupt the return and hence this is a non-linear problem and without any prior knowledge of the geo-physical parameters, it is hard to find a solution to this problem.

Conventionally, the Fourier (or Inverse Fourier) Transform algorithm is applied to the received signal (in frequency domain/time domain) signal and is converted into the range profile. This composite return may contain weaker signals from deeper layers. The major disadvantage of using Fourier transform techniques is the range side lobes, that can mask weaker reflections from deeper layers [4]. Normally, windowing functions can help reduce the side lobes of strong reflections. However the use of these windowing functions will attenuate the lower frequencies that contain most of the information about the deeper structure of the surface. Hence, it is necessary to develop a signal processing algorithm to minimize the range side lobes for enhancement of sub-surface features and then estimate the unknown parameters.

### **1.3 The Model Based Approach**

Typically Model based techniques attempt to estimate the unknown parameters by comparing the measured radar target signatures with a mathematical model such that it closely follows the underlying physical phenomenon. Figure 1-2 below depicts the model based approach to data inversion.

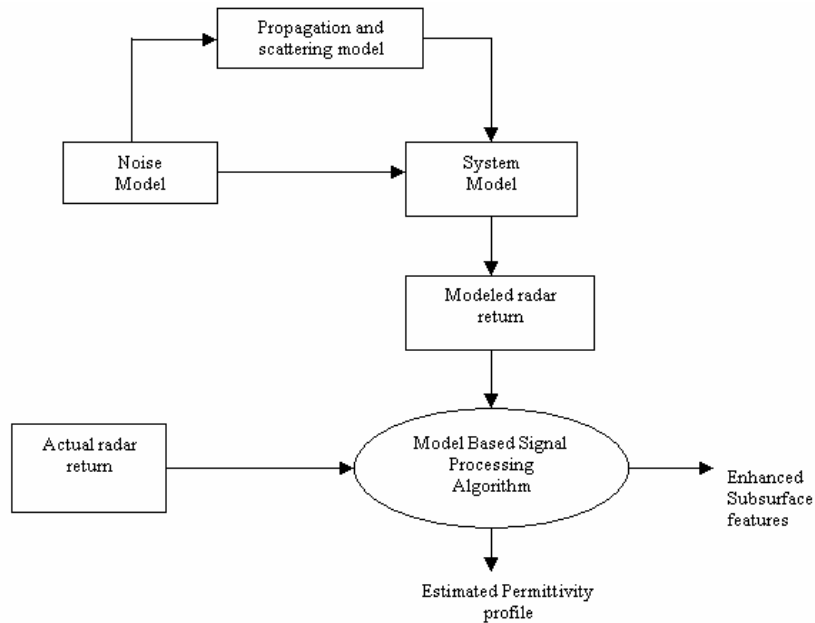


**Figure 1-2 The Model Based Approach for data inversion**

Broadly, Model Based Techniques fall under two categories – MMSE Minimization and Spectral Estimation. In the MMSE minimization approach, the unknown permittivity is estimated based on the principle of minimizing the mean square error between the measured and the modeled data. The Gauss Newton Method and Kalman Filter algorithm [5] are two well known algorithms in this category. In the spectral estimation approach, permittivity is estimated by first estimating unknown frequency components in the return signal spectrum and then estimating reflection coefficient amplitudes with a likelihood estimator. Well known spectral estimation algorithms are the Multiple Signal Classification (MUSIC) algorithm, Minimum norm algorithm and the Eigen vector algorithm. In all of these algorithms, it is necessary to have a good GPR response model (forward model) that relates model parameters to the underlying geo-physical phenomenon.

In order to model a GPR response, there are a variety of simulation methods. For a basic first order simulation, a simple convolution based modeling technique is used. For more accurate results, the effects of scattering due to random surfaces and the three dimensional antenna beam pattern can be obtained using complicated methods such as the Finite Difference Time Domain (FDTD) method, at the cost of complexity and computational time. However, in this research, we have considered the first method- The Convolution based approach for simplicity.

## **1.4 Organization**

This thesis is organized into 6 Chapters. The fundamental concepts and parameters necessary for the modeling of GPR data are discussed in Chapter 2. Chapter 3 gives an overview of the Inverse problem, the use of Model Based Techniques for Inversion, a few techniques available and a detailed analysis of a super-resolution method- The MUSIC Algorithm and its advantages over iterative MMSE minimization methods. Chapter 4 presents a few simulations for inversion on FMCW radar data and an analysis of the performance of MUSIC. Chapter 5 describes the testing of the Inversion algorithm on actual FMCW radar data collected during field experiments in Antarctica and Greenland. The algorithm was also tested in the sandbox facility of the Remote Sensing Lab (RSL) of the University Of Kansas. The results of this test are also presented. Chapter 6 describes the Graphical User Interface (GUI) developed for the Model Based Inversion. The concluding chapter summarizes our work and contains some recommendations for further research.

## Chapter 2

# Forward Modeling of radar return

---

To study any physical (or geophysical) system, the scientific procedure to be followed as given in [6] is:

1. *System parameterization*: This involves discovering the set of model parameters whose values completely characterize the system.
2. *Forward Modeling*: This involves discovering the underlying physical phenomenon and deducing a mathematical relationship between the model parameters and actual observations.
3. *Inverse Modeling*: This involves the use of the actual results of some measurements of the observable parameters to infer the actual values of the model parameters.

We first examine the mathematics of a forward model and its need. As stated in chapter 1, we are interested in estimating unknown parameters, given an observed data set. We therefore need to identify the parameters that are required. Once these parameters are identified, we can establish a mathematical relationship between the given data and the parameters to be estimated. Then, depending on the type of relationship (i.e., linear or non-linear), the inverse solution can be constructed. In this chapter, we will look at the parameters necessary to

successfully model a GPR return and derive a mathematical relationship between the known data and the unknown parameters. We now look at a case where we wish to model the returns from a multilayered target.

## 2.1 Plane wave propagation in Multi-layered Media

In modeling horizontally layered media, it is a common approach to consider plane wave approximation for EM propagation [7]. This means that it is assumed that the multiple layers are perfectly planar and that the antenna beam is like a pencil beam as shown in Figure 2-1.

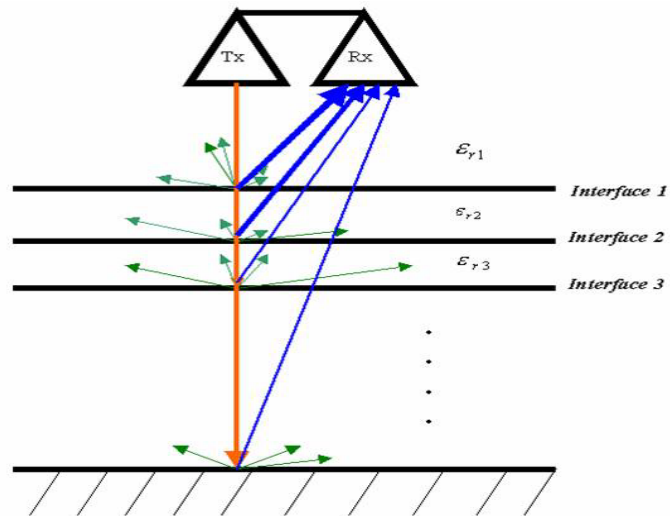


Figure 2-1 Multi-layered target with different dielectric boundaries

### 2.1.1 Permittivity

For any geo-physical phenomenon, there has to be an equivalent electrical parameter. In the case of reflected radar signals, there is an underlying fundamental

electrical parameter that is responsible for the reflection of EM waves. This parameter is called the permittivity or the dielectric constant of the material. In the field of electromagnetics, permittivity is a measure of how much a medium changes to absorb energy upon the influence of an electric field. For good dielectric materials, permittivity is a real quantity and is determined by the displacement current flowing through it. In the case of a lossy medium, conduction currents also flow through the material, and we define a complex value for permittivity [7] as

$$\epsilon = \epsilon' - j\epsilon'' \quad (2.1)$$

where  $\epsilon'$  is the real part of permittivity and it represents the capacity of the medium to store EM energy. The imaginary part of permittivity,  $\epsilon''$  represents the EM energy losses [7] (due to absorptive properties of the medium). In general, permittivity is a function of frequency, but for the purposes of simplicity, we will assume a *frequency-independent* situation for our problem.

Every material on earth has a unique value of permittivity. If not for the concept of permittivity, we wouldn't be able to distinguish between ice, water and snow, which are just different forms of the same material. Ice has a permittivity of around 3.14, it is around 80 for water, and for snow, it can vary depending on its density and moisture content. Hence, the underlying permittivity is responsible for each of these materials interacting in a different way with the same incident EM wave. As will be seen in the next chapter, radars exploit this phenomenon and are successfully being used in remote sensing to characterize materials.

## 2.2 Wave Propagation Phenomena

When EM wave propagating down strikes layers of differing dielectric constants, the following phenomena occur:

### 2.2.1 Reflection & Transmission

Whenever an EM wave encounters a dielectric interface, a part of the incident signal is reflected back to the source and a part of it propagates into the layer. The reflected signal amplitude is proportional to the reflection coefficient at the dielectric interface defined as the ratio of the positive directed field divided by the negative directed field or alternatively, the ratio of the reflected wave divided by the incident wave. In mathematical terms, the reflection coefficient denoted by  $\Gamma_k$  is defined [7] as:

$$\Gamma_k = \left( \sqrt{\epsilon_{k+1}} - \sqrt{\epsilon_k} \right) / \left( \sqrt{\epsilon_{k+1}} + \sqrt{\epsilon_k} \right) \quad (2.2)$$

where  $\epsilon_k$  is the permittivity of layer k and  $\epsilon_{k+1}$  represents the permittivity of the next layer. The portion of the EM wave transmitted can be derived recognizing the boundary condition at the interface, by which the sum of the power transmitted ( $P_T$ ) into the layer and that reflected ( $P_\Gamma$ ) from the layer is equal to one, i.e.,  $P_T + P_\Gamma = 1$ , where

$$P_{\Gamma,k} = |\Gamma_k|^2 \quad (2.3)$$

If we define the transmission coefficient at layer  $k$  as  $T_k$ ,

$$P_{T,k} = |T_k|^2 \quad (2.4)$$

the value of reflection coefficient will be

$$T_k = \sqrt{1 - |\Gamma_k|^2} \quad (2.5)$$

which then yields

$$T_k = \sqrt{4\sqrt{\epsilon_k \epsilon_{k+1}} / [\sqrt{\epsilon_{k+1}} + \sqrt{\epsilon_k}]^2} \quad (2.6)$$

Hence, a positive value of reflection coefficient indicates an increasing dielectric profile and a negative value indicates a decreasing profile at the interface.

## 2.2.2 Attenuation

As seen earlier, EM energy returns to the radar because of reflection. However, part of the EM energy that is not reflected propagates further into medium and can get attenuated. Given below are some of the phenomena that may attenuate an EM signal.

### 2.2.2.1 Scattering

Scattering is a phenomenon that occurs due to the interaction of EM waves with irregular (rough) surfaces. Hence we have the concept of *Surface scattering*. A signal ray incident normally on this rough surface does not undergo specular reflection. Instead, it is scattered in different directions and causes a reduction in

return signal. The signal loss is usually a function of the Root Mean Square (RMS) surface height. To account for the attenuation due to surface scattering, we are required to model this effect. Commonly used are the Kirchoff Approximation and Geometric optics models. But, for simplicity, a generally accepted technique is to account for roughness by approximating surface and sub-surface layers by a Gaussian random variable that incorporates the randomly varying height profile. The average impulse response of the surface in the form of a Gaussian specular point-density function [8] is given by equation 2.7 below.

$$h(\tau) = \frac{1}{\sqrt{2\pi\left(\frac{2\sigma_s}{c}\right)^2}} \exp\left[-\frac{\tau^2}{2\left(\frac{2\sigma_s}{c}\right)^2}\right] \quad (2.7)$$

where  $\sigma_s$  is the rms variation of surface height,  $\tau$  is the time delay variable corresponding to the two way distance traveled by the signal,  $c$  is the velocity of the EM wave.

The second type of scattering is called *Volume Scattering*. Volume scattering occurs because the multiple target layers are not homogenous. Rather, the layers are a mixture of particles suspended in a background medium. For example, snow can be considered as ice suspended in a background medium of air. Particles of ice scatter the incident signal in all directions. This phenomenon further causes loss of signal and needs to be accounted for. Generally, the loss due to volumetric scattering is modeled by a “Volumetric scattering coefficient” which is a function of the volume

of the suspended medium, volume of the background medium and the number of scattering particles per unit volume [9].

### 2.2.2.2 Absorption

Certain materials have the property of absorbing EM radiation when incident on them. Hence, the EM wave is attenuated. From an electrical point of view, we normally include an “Absorption coefficient” to model the attenuation due to absorption [10]. This coefficient depends on the particle size, wetness percentage, type of background material, etc.

### 2.2.2.3 Spreading

Due to the antenna beam pattern, the signal transmitted through the atmosphere experiences a loss in power at a rate inversely proportional to the distance travelled. If a signal with power  $P_t$  is transmitted by an antenna having gain  $G_t$ , the power at a distance  $R$  from the antenna is given by

$$P_r = P_t G_t \left( \frac{1}{4\pi R^2} \right) \quad (2.8)$$

The term in brackets is called *Free space spreading loss* due to the shape of the antenna beam. Hence, for a two way distance of  $2R$ , there is a loss of  $\left( \frac{2}{4\pi R^2} \right)$  due to spreading.

## 2.3 Modeling Target Response

If all of the above factors can be accurately determined, we can essentially construct the radar return using simulations. This is called the *Forward Modeling* of

radar signal. So far, we looked at various factors that can influence radar return and their mathematical interpretation. Now, we will look at combining all these factors to model the overall composite signal that reaches the radar receiver. Figure 2-2 below gives a simplified notion of the discussion thus far.

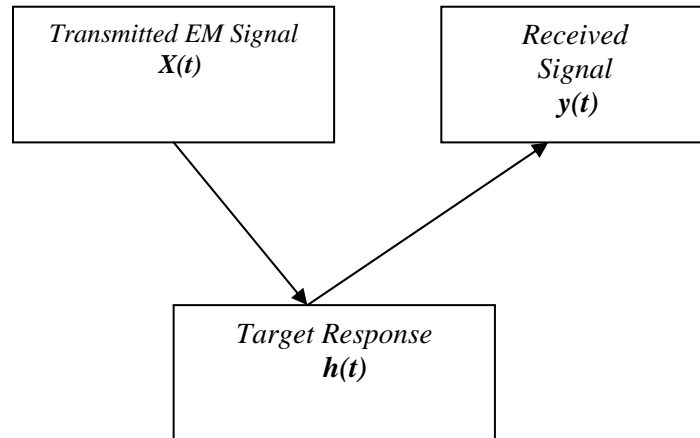


**Figure 2-2 Block diagram of the forward modeling problem**

The response of a system to an impulse is called the *Impulse Response* of the system. The impulse response of a multi-layered target can be modeled from its contributing parameters discussed above. In order to model the physical phenomenon, a widely accepted method is the *Convolution-Based* scheme based on one dimensional modeling [4]. This means that, if we denote the transmitted signal as  $x(t)$  and the target response as  $h(t)$ , then the received radar signal is simply the convolution of  $x(t)$  and  $h(t)$ . This is based on the assumption that plane wave propagation or ray propagation model holds good to represent the phenomenon. Convolution in the time domain corresponds to multiplication in the frequency domain. Hence, we can also write:

$$Y(f) = H(f) \cdot X(f) \quad (2.9)$$

where each of these terms represents the transfer function of its corresponding impulse response. A graphical illustration of the overall forward modeling problem [11] is presented in figure 2-3.

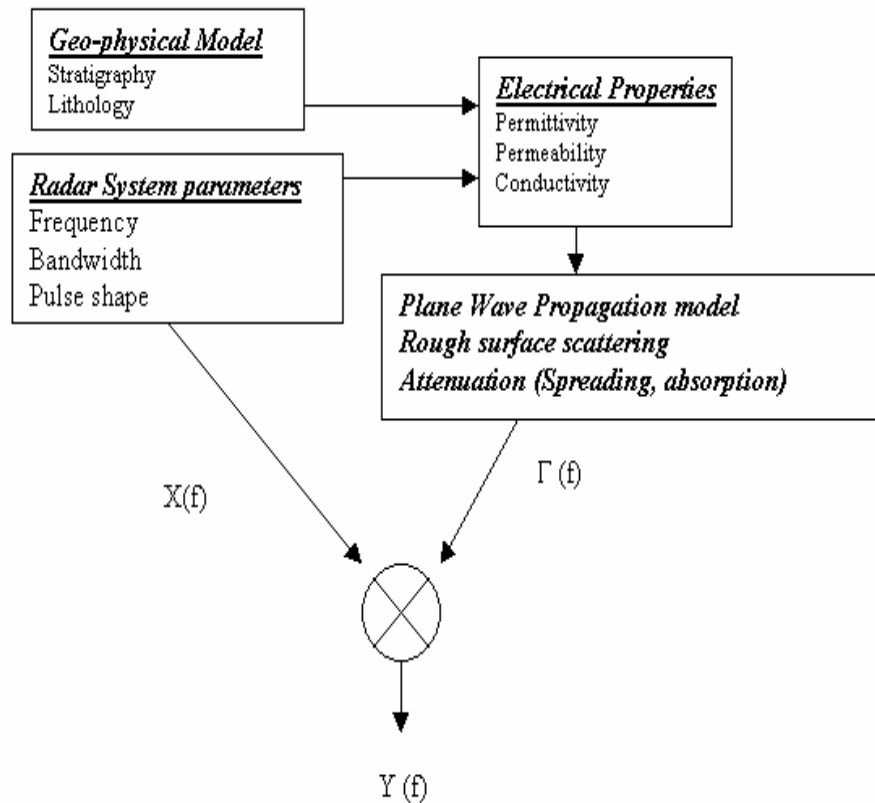


Figure 2-3 Simulation Flowchart

The RSL radar simulation package [12] based on theoretical models in [9,10] gives a good overview of the forward modeling problem and discusses various models used to simulate radar return responses for different types of propagating media.

## 2.4 Three Dimensional FDTD modeling

In the discussion so far, we have assumed a plane wave propagation model or a two-dimensional approximation of the three-dimensional phenomenon of EM wave propagation. Though this approximation can serve as a good starting point for modeling studies and inversion techniques, it cannot accurately model an actual radar target response. A much sophisticated technique is called the FDTD or Finite Difference Time domain technique of simulating three-dimensional phenomenon by implicitly including additional electromagnetic phenomena such as multiple reflections, interferences, geometrical spreading, ray focusing, phase shifts, etc., which are ignored by the convolution model seen earlier [13]. The numerical model is based on an FDTD set of Maxwell's curl equations implemented on a staggered grid with absorbing boundary conditions.

However the performance of FDTD forward modeling requires a huge number of model points and computing time, complicating simple implementation. Hence, in this thesis we will focus on the convolution model for simplicity.

## 2.5 Summary

In this chapter, the forward modeling problem was discussed, which involved converting geophysical parameters into electrical parameters (by applying appropriate models from the literature) and then forming a mathematical expression for the response of the target assuming a horizontally layered profile. In the next chapter, we will look at the inverse problem.

# Chapter 3

## The Inverse Problem

---

### 3.1 Parameter Estimation

In the previous chapter, we discussed the forward modeling problem where a mathematical model is used to represent a physical phenomenon using model parameters such as permittivity, target distance, transmit power, antenna gain, etc. We now proceed to discuss the *Inverse Problem* – which means to estimate the values of model parameters from the measured data.

Inverse permittivity profiling is one such problem where the unknown parameter (permittivity) needs to be estimated from the received radar data. More specifically, for our research, we are interested in estimating unknown permittivity values given the data measured by a GPR. This problem is called *Electro-Magnetic Inversion* or *EM parameter Estimation*. There are several parameter estimation methods; however each of these methods is applicable only to certain types of inversion problems. In this chapter, we will explore some of the existing methods and their relative merits and demerits.

Several problems in data inversion deal with estimating parameters based on continuous-time signals. However, modern radar systems use digital computers to sample and store analog waveforms, and hence we have the equivalent problem of extracting parameter values from a discrete time waveform or a discrete data set [14].

Mathematically, let us assume that the data set  $Y = \{y[0], y[1], \dots, y[N-1]\}$  represents the sampled version of the observed data, where  $N$  is the number of samples in the waveform. This data set depends on an unknown parameter  $m$  and we wish to determine the set of values  $m$  based on the data set  $Y$  or, equivalently, we wish to define an estimator [6,15]

$$\hat{m} = G(y[0], y[1], \dots, y[N-1]) \quad (3.1)$$

where  $G$  is some function. This is called the general *Parameter Estimation* problem from a mathematical perspective. For our remote sensing problem, the data set denoted by  $Y$  is the data obtained from a GPR;  $\hat{m}$  translates into the set of permittivity values  $\hat{\epsilon}$  (permittivity profile) that we wish to estimate. To determine a good estimator, the first step is to mathematically model the data. From chapter 2, we have a forward model, denoted by  $F(m)$  which relates the actual model parameters ( $m$ ) to the composite target response. Mathematically,  $F$  may be a linear or a non-linear function in  $m$ . However, the signal that reaches the radar receiver is not just the planar target response, but also a sum of the target response, noise and other errors which can be systematic or random. Hence, we can write the total observed data set as [6,15] :

$$Y(n) = F(m, n) + n + S \quad (3.2)$$

where  $n$  denotes additive white Gaussian Noise (AWGN) and  $S$  denotes systematic or random errors which clutter the total signal returned to the radar

receiver. For the radar problem,  $\mathbf{n}$  could represent thermal noise and quantization errors.  $\mathbf{S}$  can be used to represent system non-linearities and returns due to clutter. Before proceeding to estimate  $\mathbf{m}$  given  $\mathbf{Y}$ ,  $\mathbf{S}$  needs to be eliminated from the observed data by suitable calibration techniques. We are now left with the problem of estimating  $\mathbf{m}$  from data corrupted by white Gaussian Noise. We will now look at a few techniques that attempt to meet our objectives.

## 3.2 Inversion by Layer Stripping

Layer stripping [16] is an elementary approach for data inversion. Continuing the discussion in the previous section, let us assume that we have eliminated clutter from the observed data. Hence, ideally, we are left with a delayed and attenuated version of the transmitted signal. As mentioned earlier, the Fast Fourier Transform (FFT) algorithm is applied on the received waveform to obtain the spectrum of the signal. A plot of this signal with respect to the distance axis will show the occurrence of sharp peaks at interface locations. Ideally, the amplitudes of these peaks will correspond to the reflection coefficients (and transmission coefficients) at their respective interface locations. That is, the amplitude of reflected signal at any layer  $\mathbf{k}$  is given by equation 3.3 as

$$\mathbf{A}_k = \mathbf{B}_k \sum_{k=1}^L \Gamma_k \prod_{j=1}^k \mathbf{T}_j \quad (3.3)$$

where  $\mathbf{B}_k$  represents the attenuation coefficient, which accounts for losses due to absorption, scattering and spreading. However, modeling the attenuation coefficient

requires some *a priori* information regarding the properties of the target. Hence, for our inversion problem, we will assume that the lossy part of the medium (which contributes to the attenuation coefficient) is known. We also assume that the transmission coefficient for the first layer (air)  $\mathbf{T}_1 = \mathbf{1}$ . The “ideal” amplitude of the surface reflection will be  $\Gamma_1 \mathbf{T}_1$ , the subsequent layers will have amplitudes  $\Gamma_2 \mathbf{T}_1 \mathbf{T}_2$ ;  $\Gamma_3 \mathbf{T}_1 \mathbf{T}_2 \mathbf{T}_3$  and so on. The locations of their corresponding distances are directly related to their respective time delays. If  $Z_0$  represents the height of the surface from the antenna and  $Z_k$  represents the depth of the  $k^{\text{th}}$  layer in a multi-layered media of  $\mathbf{L}$  layers, the two-way time delay  $\tau_k$  experienced by the signal is given as

$$\tau_k = \frac{2}{c} \left[ z_o + \sum_{i=1}^k (z_i - z_{i-1}) \sqrt{\epsilon_i} \right] \quad (3.4)$$

The idea in layer stripping is that we first identify the amplitudes ( $\mathbf{A}_k$  's) and the locations of interfaces ( $\tau_k$  's) from the range profile of the received signal. Once these values are known, it is easy to determine unknown variables (permittivity values) recursively using equations (3.3) and (3.4).

The first task is the detection of echoes. This is done by setting a reasonable threshold amplitude value based on the Signal-to-Noise ratio (SNR) of the system. All amplitudes that cross this threshold are picked as valid returns. The positions

corresponding to these returns constitute the distances (delays). These values are used to recursively estimate the permittivities.

However, since the detection of echoes is performed without any reference to a geophysical model, this approach suffers from the following limitations.

1. **Missed Peaks:** Since the detection of echoes is done by setting a threshold by looking at the range profile, the value of the threshold is important. In certain profiles consisting of small dielectric variations, the reflection at that interface could be very small and could be embedded in noise. Hence, without any knowledge of the profile, an arbitrary threshold value might cause missing of that peak. Hence, this leads to an error in the estimated permittivity profile.

2. **False Alarms:** In many cases, we might not be able to distinguish between actual signal peaks and false alarms – which are unwanted reflections that arise due to the presence of random noise or reflections due to clutter/external factors. The selection of false alarms as signal peaks can also lead to erroneous permittivity profiles.

3. **Range Sidelobes:** To obtain the range profile, the Fourier transform algorithm is usually applied on the IF beat signal measured by an FMCW radar. But, this method suffers from the problem of range sidelobes. That is, the weaker reflections (smaller reflection coefficients) are masked by the sidelobes of stronger reflections. Hence, this presents a serious impediment when identifying valid peaks from the range profile for data inversion.

Hence, we find the need for a more robust parameter estimation algorithm – preferably one which incorporates the underlying physical phenomenon. In chapter 4,

we will present simulations using the layer stripping technique and demonstrate cases where they can successfully invert the data and also cases where they suffer from the limitations as discussed earlier.

### 3.3 Model Based Estimators

Stergiopoulos [17] suggests that, if the physical phenomenon is incorporated into the algorithm, the inversion results are better. Such an estimator, which uses the geophysical model to estimate unknown parameters is called a *Model Based Estimator*.

Let us revisit equation (3.2) which gives a mathematical relationship between the observed data and the model parameters by a forward model  $\mathbf{F}$ . Typically, in radar problems, the function  $\mathbf{F}$  is non-linear. Therefore, our objective is to find a model-based non-linear estimator of  $\mathbf{m}$ . This problem is also called *fitting of a nonlinear regression model*. Kay [14] suggested the use of Minimum variance unbiased (MVU) estimators for such a problem. By unbiased estimators, we mean that on the average, the estimator will yield the true value of the unknown parameter or the MVU estimator is the one which provides an optimum estimate of the unknown variables, at the same time exhibiting the minimum variance. However, these estimators require probabilistic assumptions about the observed data, or in other words, the estimator produces an unbiased output only when the Probability Density Function (PDF) of the data can be sufficiently determined. This can be possible only

in the absence of error components in the data. Hence we conclude that, in radar problems, MVU estimators cannot yield good estimates.

This led to the development of Model-based algorithms which use different criteria for parameter estimation. Extensive literature search showed that two classes of algorithms could be used for inversion on GPR data. These model based approaches explored in this research are:

1. *MMSE (Minimum Mean Squared Error) Minimization* – which is based on the least squares approach of minimizing the mean squared error between the observed data and the model.
2. *Spectral Estimation* – This is based on estimating model parameters by first estimating the frequency components in the signal spectrum and then using the model to invert the observed data. A detailed view of both these methods is presented next.

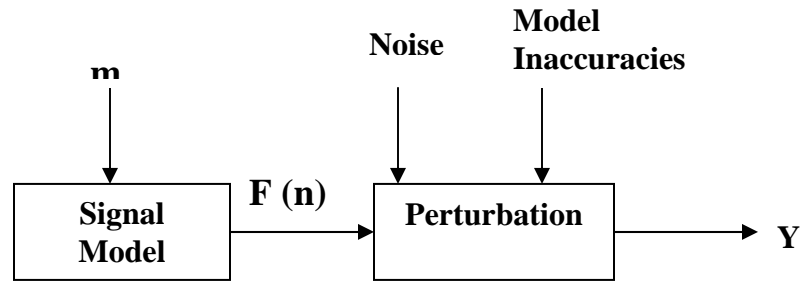
### **3.3.1 MMSE Minimization Algorithms**

The MMSE approach dates back to 1795 when the famous scientist Gauss used the method to study planetary motions [18]. In this method, we attempt to minimize the squared difference between the observed data  $\mathbf{Y}$  (given by equation 3.2) and the assumed signal model or noiseless data  $\mathbf{F}$ , which is a function of the unknown parameter  $\mathbf{m}$ . This concept is illustrated in Figure 3-1 [14].

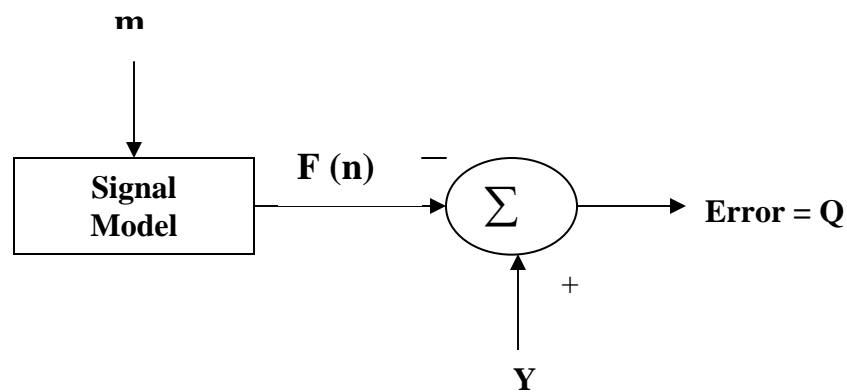
A fundamental assumption in this approach is that the signal  $\mathbf{F}(\mathbf{m}, \mathbf{n})$  is purely deterministic. As discussed earlier, due to random noise or model

inaccuracies, we observe a perturbed version of  $F(m, n)$ , which is denoted as  $Y$ .

The MMSE estimator of  $m$  chooses the value that makes  $F(m, n)$  closest to the observed data  $Y(n)$ .



(a) Data Model



(b) Least Squared error

Figure 3-1 The Least Squares Approach

Closeness is quantified by the least squared error criterion given by equations (3.5) and (3.6) below

$$Q = \sum_{n=0}^{N-1} (Y(n) - F(m, n))^2 \quad (3.5)$$

OR

$$Q = \|Y(\mathbf{n}) - F(\mathbf{m}, \mathbf{n})\|^2 \quad (3.6)$$

where the observation interval is assumed to be  $\mathbf{n} = \mathbf{0}, \mathbf{1}, \dots, \mathbf{N}-\mathbf{1}$ . The value of  $\mathbf{m}$  that minimizes  $Q$  is the MMSE estimator of  $\mathbf{m}$ . The performance of this method depends upon the properties of the corrupting noise as well as other external and internal sources of error in the system and in the observation. We will now explore two of the popular MMSE type inversion methods – the Gauss Newton Method and the Kalman filter method.

### 3.3.1.1 Gauss Newton Method

As mentioned earlier, there is a non-linear relationship between the signal model and the model parameters. It is well known that non-linear least squares problems are difficult to solve. They must first be converted into linear form. The iterative Gauss Newton method [16] gives a solution by linearizing the model  $F(\mathbf{m}, \mathbf{n})$  about some nominal  $\mathbf{m}$  and then uses the linear least squares procedure as described in [14,16].

$$F(\mathbf{m}) \cong F(\mathbf{m}_c) + [\nabla_{\mathbf{m}} F(\mathbf{m}_c)](\mathbf{m} - \mathbf{m}_c) \quad (3.7)$$

where  $\nabla_{\mathbf{m}} F(\mathbf{m}_c)$  indicates the matrix of partial derivatives of  $F(\mathbf{m})$  with respect to model parameters evaluated at  $\mathbf{m} = \mathbf{m}_c$ . The variable  $\mathbf{m}_c$  - which denotes the set of

current model parameters. Revisiting equation (3.4), we can derive the solution of the non-linear problem as follows.

$$Q = \sum_{n=0}^{N-1} (Y(n) - F(m, n))^2 \quad (3.8)$$

$$\approx \sum_{n=0}^{N-1} \left( Y(n) - F(m, n) + \frac{\partial F[m, n]}{\partial m} \Big|_{m=m_0} m_0 - \frac{\partial F[m, n]}{\partial m} \Big|_{m=m_0} m \right)^2 \quad (3.9)$$

To initiate the algorithm, we begin with a starting guess for the model parameters, denoted by  $m_0$ . Proceeding further, equation (3.8) can be written as

$$Q = \left[ Y - F(m_0) + H(m_0)m_0 - H(m_0)m \right]^T * \left[ Y - F(m_0) + H(m_0)m_0 - H(m_0)m \right] \quad (3.10)$$

where we define  $\mathbf{H}$  as the matrix of partial derivatives of the modeled data with respect to the model parameters  $\mathbf{m}$ . Now since we have a linear model, we can use the theory of least squares error minimization [15] where the model updating is obtained by back projecting the residual i.e.,  $Y - F(m)$  onto the model space to obtain the solution. Equation (3.9) can be solved to obtain the Least square error estimate as:

$$\hat{m} = \left[ H^T(m_0)H(m_0) \right]^{-1} H^T(m_0) \left[ Y - F(m_0) + H(m_0)m_0 \right] \quad (3.11)$$

$$= m_0 + \left[ H^T(m_0)H(m_0) \right]^{-1} H^T(m_0) \left[ Y - F(m_0) \right] \quad (3.12)$$

This can be iterated so that

$$m_{k+1} = m_k + \left[ H^T(m_k)H(m_k) \right]^{-1} H^T(m_k) \left[ Y - F(m_k) \right] \quad (3.13)$$

The implementation details of this algorithm are presented in chapter 4.

### ***3.3.1.1.1 Limitations of the Gauss-Newton Technique:***

Now, we will look at common problems encountered when fitting nonlinear regression models.

#### **Convergence Issues:**

Methods of parameter estimation like the Gauss-Newton MMSE algorithm and MVU estimate algorithm which are iterative procedures suffer from convergence problems. As discussed earlier, the algorithm produces an estimate  $\hat{\mathbf{m}}$  that minimizes the mean squared difference  $Q$  between the observed and the model parameters. To find the optimum estimate, the algorithm is initiated with a starting guess  $\mathbf{m}_0$  or, for convenience  $\mathbf{m}^{(1)}$  and then sequentially find  $\mathbf{m}^{(2)}, \mathbf{m}^{(3)}, \dots$  in such a way that the sequence finally converges to  $\hat{\mathbf{m}}$  - which yields the minimum mean squared error. This process is called convergence and the value of MMSE obtained is called the *Global minimum*.

In simple mathematical terms, a global minimum of a function is the lowest value that the function achieves. In our case, this function is the error function that we are trying to minimize. If we assume the function to be a surface, then a Global minimum is the lowest point on that surface. MMSE minimization algorithms are typically based upon a quadratic approximation to the error function  $Q(\mathbf{m})$ . Seber [15] suggests that the Newton method will converge provided the starting guess  $\mathbf{m}^{(1)}$

is close enough to the estimate  $\hat{\mathbf{m}}$ . However, in a few cases, global minimum convergence is not achieved. The algorithm could result in a *local minimum*. The local minimum of a function is a point which has a value lesser than all points next to it. Using the example of a surface, a local minimum is the bottom of a valley or a bowl in the surface somewhere. Figure 3-2 below depicts this concept [19].

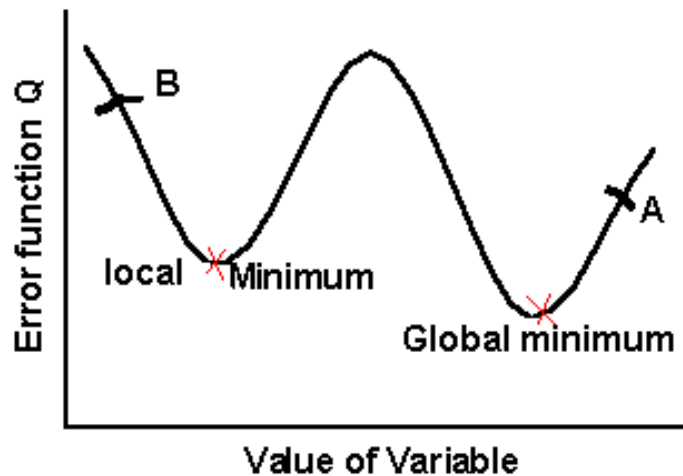


**Figure 3-2 The concept of Local and Global minimum**

If this guess  $\mathbf{m}^{(i)}$  is close to point B in the above figure, then the convergence is most likely local and when  $\mathbf{m}^{(i)}$  is around point A, then the algorithm will yield a global minimum value.

Apart from the problem of local minimum convergence, MMSE methods at times, do not converge at all. Again, as in the local minimum case, convergence is sensitive to the starting guess. A bad starting value ( $\mathbf{m}^{(i)}$ ) can either result in a local minimum or may never converge at all. However, MMSE minimization techniques are still widely used to solve non-linear problems because they can fit a broad range

of functions. Also, they produce good estimates of the unknown parameters in the model with relatively small data sets [14].

A simple, but time consuming approach to circumvent the problem of convergence is to run this algorithm with several starting guess values and select the case with the least error. Also, the model parameter values at every iteration need to be constrained and should not be permitted unlimited freedom of movement. A few methods of constrained optimization for non-linear regression are available in [15,20].

#### **Discretization of depth:**

The first step in implementing the Gauss Newton method is the parameterization of permittivity with depth. This means that we first reduce the estimation problem to the necessary number of unknown parameters and decide the depth sampling constant based on the overall depth of the profile and on the range resolution of the radar so that the locations of dielectric interfaces can be identified. Minimization algorithms frequently run into the problem of producing useless solutions [16] when the true depths are not an integer multiple with depth sampling. For approximate depth sampling values, the algorithm gives a perturbed set of parameter values. More specific details on the implementation of the Gauss Newton method and its limitations will be presented through simulations in the next chapter.

#### **3.3.1.2 Kalman Filter Method**

Diverging a little bit from the classical approach to statistical parameter estimation, where the parameter of interest  $\mathbf{m}$  is assumed to be a deterministic

quantity embedded in random noise, the Bayesian approach assumes that the unknown parameter  $\mathbf{m}$  is a random variable whose particular realization we are required to estimate. Bayesian estimators fall under two categories: MMSE based estimators and maximum a posteriori estimators [21]. The extended Kalman Filter is a type of non-linear Bayesian estimator. Before we go into the details of the Kalman filter, let us look at dynamic signal models for Bayesian estimators. A dynamic signal can be modeled as:

$$\mathbf{Y}(n) = \mathbf{F}(\mathbf{m}[n]) + \mathbf{w}(n) \quad (3.14)$$

where  $\mathbf{Y}(n)$  refers to the observed data samples;  $\mathbf{F}(\mathbf{m}[n])$  represents the transformation from the state variables (or the vector model parameter variable  $\mathbf{m}$ ) to the ideal observations (without noise).  $\mathbf{w}(n)$  represents zero mean additive white Gaussian noise with independent samples. The state equation for the extended Kalman filter is:

$$\bar{\mathbf{m}}(n) = \bar{\mathbf{m}}(n-1) + \mathbf{u}[n] \quad (3.15)$$

where  $\mathbf{u}[n]$  accounts for modeling errors and unforeseen inputs. The non-linear model  $\mathbf{F}(\mathbf{m}, n)$  has to be linearized using the Gauss Newton approach discussed earlier. More specific details on the implementation of the Extended Kalman Filter are given in [14]. The performance of the Kalman filter is very sensitive to the accuracy of the linearization operation and hence, this approach too suffers from the problems discussed in the earlier section.

### 3.3.2 Spectral Estimation Techniques

Spectral estimation deals with estimating the frequency components (or spectral components) of a signal given a noisy measurement. So, the question that comes up is - How is this method related to parameter estimation? In many problems that deal with parameter estimation, the spectral components that make up the frequency response of the cumulative radar return are related to the time delays experienced by EM waves as they strike dielectric interfaces. Once we estimate the individual delays, the reflection coefficients can be estimated using a maximum likelihood estimator and eventually, the permittivity profile can be reconstructed.

To estimate the power spectrum of a process, typically, the power spectral densities need to be known. However, as in our problem of noisy radar data, this information is not available. The power spectrum needs to be estimated from the observation of the process itself.

The simplest example of spectral estimation of a random process is the fast Fourier transform or the FFT. But as seen earlier, the range side lobes associated with the FFT pose a serious challenge in resolving reflections from weak reflecting boundaries. To be more precise, the deeper reflections from dielectric interfaces are weak and they get buried under the side lobes of stronger reflections and hence, the Fourier transform method does not provide a high-resolution estimate of the underlying spectrum. However, if this random process can be modeled, then the

spectrum may be estimated with the use of high resolution spectral estimation techniques.

Broadly, there are two approaches for spectral estimation : Non- Parametric and Parametric approach. In the classical Non-parametric approach, the power spectrum is estimated by taking the Fourier transform of the autocorrelation sequence of the given measurement. However, the limitation with the non-parametric approach is that they are not designed to incorporate *apriori* information about the process into the estimation procedure. Hayes [21] suggested that incorporating a model for the process into the spectral estimation algorithm yields a more accurate and higher resolution estimate of the spectral components. This leads us to the parametric approach.

In the parametric approach to spectral estimation, the first step is to select an appropriate model for the process. This could be based on apriori knowledge about how the process is generated or on experimental results, which fit a model to the observation. Commonly used models include the Autoregressive model (AR), Moving average model (MA), autoregressive moving average (ARMA) and harmonic models. Once the model has been decided, the next step is to estimate the model parameters from the given data. The last step is to estimate the power spectrum by incorporating the estimated parameters into the parametric form of the spectrum.

The nature of our problem suggests the use of harmonic model. This means that we can consider the problem of radar signal detection as an equivalent problem

of estimating unknown frequencies (that correspond to specific layers) from a composite radar return signal corrupted by noise.

Let us consider  $x(\mathbf{n})$  to be the return signal, which is the sum of complex exponentials in noise. Equation 3.16 below defines this idea mathematically

$$x(\mathbf{n}) = \sum_{i=1}^p A_i e^{jn\omega_i} + w(\mathbf{n}) \quad (3.16)$$

where  $A_i = |A_i| e^{j\phi_i}$  represents the complex amplitude of the  $i^{\text{th}}$  sinusoid in the composite signal;  $\phi_i$  represents an uncorrelated random variable uniformly distributed over the interval  $[-\pi, \pi]$ . From the standpoint of our problem, the known quantity is the received signal and the unknown terms are the frequencies  $\omega_i$  and magnitudes  $A_i$  of the complex exponentials in  $x(\mathbf{n})$ . Thus, the power spectrum of  $x(\mathbf{n})$  consists of a set of  $p$  sinusoids at frequencies  $\omega_i$  in addition to the power spectrum of additive noise  $w(\mathbf{n})$ . Typically, the complex exponentials are the information bearing part of the signal and we are interested in estimating the frequencies and amplitudes rather than the power spectral density. Estimation of unknown parameters using spectral estimation techniques involves :

1. Finding the auto-correlation matrix of  $x(\mathbf{n})$  denoted by  $\mathbf{R}_x$
2. Eigen decomposition of  $\mathbf{R}_x$  into two sub-spaces : the signal subspace and the noise subspace.

### 3. Estimation of unknown frequencies by evaluating a frequency estimation function

Some of the popularly available estimation methods that can be used for parameter estimation are discussed in the following sub-sections.

#### 3.3.2.1 The MUSIC Algorithm

Schmidt [22] came up with a super-resolution frequency technique called MUSIC, which stands for **M**ultiple **S**ignal **C**lassification. This method is an extension of the Pisarenko Harmonic Decomposition method [21] which works on the principle that it is possible to estimate unknown sinusoidal components in noise from the eigenvector corresponding to the minimum eigenvalue of the autocorrelation matrix by exploiting the orthogonality of signal and noise.

To better understand how the algorithm works, let us first assume a random process that consists of a single complex exponential in white noise. As per the signal model defined earlier,

$$\mathbf{x}(\mathbf{n}) = A_1 e^{jn\omega_1} + w(n) \quad (3.17)$$

where  $A_1$  is the amplitude of the complex exponential and the other terms carry the same meaning as defined earlier. The autocorrelation sequence of  $\mathbf{x}(\mathbf{n})$  is

$$r_x(k) = P_1 e^{j\omega_1 k} + \sigma_w^2 \delta(k) \quad (3.18)$$

where  $P_1$  is the power in the complex exponential. The autocorrelation matrix for  $x(\mathbf{n})$  is just a sum of the autocorrelation matrix due to the signal,  $R_s$ , and the autocorrelation matrix due to the noise  $R_n$ . Therefore, we have

$$R_x = R_s + R_n \quad (3.19)$$

The signal autocorrelation matrix can be represented as:

$$R_s = P_1 \begin{bmatrix} 1 & e^{-j\omega_1} & e^{-j2\omega_1} & \dots & e^{-j(M-1)\omega_1} \\ e^{j\omega_1} & 1 & e^{-j\omega_1} & \dots & e^{-j(M-2)\omega_1} \\ e^{j2\omega_1} & e^{-j\omega_1} & 1 & \dots & e^{-j(M-3)\omega_1} \\ \vdots & \vdots & \vdots & \ddots & \vdots \\ \vdots & \vdots & \vdots & \ddots & \vdots \\ e^{j(M-1)\omega_1} & e^{j(M-2)\omega_1} & e^{j(M-3)\omega_1} & \dots & 1 \end{bmatrix} \quad (3.20)$$

and the noise autocorrelation matrix  $R_n$  is a diagonal matrix of full rank.

$$R_n = \sigma_w^2 I \quad (3.21)$$

Clearly,  $R_s$  is a matrix of rank one and has only one non-zero eigen value. It follows that the signal eigen vector is

$$e_1 = [1, e^{j\omega_1}, e^{j2\omega_1}, \dots, e^{j(M-1)\omega_1}] \quad (3.22)$$

The signal autocorrelation matrix can be represented as:

$$R_s = P_1 e_1 e_1^H \quad (3.23)$$

This yields the non zero eigen value of the signal to be  $M P_1$ . Also, it can be seen that the matrix  $R_s$  is Hermitian. Hence, we can say that the remaining eigen vectors  $v_2, v_3, \dots, v_M$  will be orthogonal to  $e_1$ .

$$e_1^H v_i = 0; \quad i = 2, 3, \dots, M \quad (3.24)$$

This is called the *Orthogonality condition*. The same concept can be extended to two complex exponentials in noise and so on. For the case of two complex exponentials,  $R_s$  has two non-zero eigen values and hence, the first two eigen values of  $R_x$  are greater than  $\sigma_w^2$ , the variance of noise. Thus, for any number of complex exponentials, the eigen values and eigen vectors can be divided into two groups – the first group consisting of those eigenvectors whose eigen values are greater than  $\sigma_w^2$  - called the *Signal Subspace* and the second group, consisting of eigenvectors whose eigen values are equal to  $\sigma_w^2$  - referred to as the *Noise Subspace*. The eigen vectors form an orthonormal set since the autocorrelation matrix is Hermitian. Therefore, the signal and noise subspaces are orthogonal.

For MUSIC to work properly, we need many instances (return signals) of a radar measurement and the individual returns need to be uncorrelated. However, in many cases, the data obtained using a radar is coherent- this means that the signal components do not change between samples and hence the received signals need to be decorrelated. Yamada [23] suggested the use of Spatial smoothing pre-processing (SSP) to decorrelate the individual returns.

The SSP method uses an alternative data correlation matrix  $\mathbf{R}_{\text{SSP}}$  instead of the autocorrelation matrix  $R_x$  of the composite return ( signal & noise). Let us assume that we have  $L$  samples of measured data. These  $L$  samples are divided into  $M$  overlapping subarrays and  $\mathbf{r}_k$  denotes the data vector corresponding to the  $k^{\text{th}}$  subarray (where  $k= 1,2,3,\dots M$ ). We define a correlation matrix  $\mathbf{R}_k$  as:

$$\mathbf{R}_k = \frac{1}{P} \sum_{p=1}^P \mathbf{r}_k^{(p)} \mathbf{r}_k^{(p)H} \quad (3.25)$$

where  $p = 1,2,\dots P$  and  $P$  is the number of snapshots of the measurement. The data correlation matrix  $\mathbf{R}_{\text{SSP}}$  can then be written as

$$\mathbf{R}_{\text{SSP}} = \frac{1}{M} \cdot \sum_{k=1}^M \mathbf{R}_k \quad (3.26)$$

Now, the eigen value decomposition of this matrix can be performed to yield the eigen vectors denoted by  $\mathbf{e}^i$  and their corresponding eigen values denoted by  $v^i$ . Following the earlier discussion, the eigen values can then be divided into two groups :  $M$  Signal eigen vectors and  $M - p$  Noise eigen vectors, where  $\mathbf{R}_{\text{SSP}}$  is of size  $M \times M$ . If we compute the Fourier transform of the coefficients in  $v_i$ ,

$$v_i(e^{j\omega}) = \sum_{k=0}^{M-1} v_i(k) e^{-jk\omega} ; i = p+1, p+2, \dots, M \quad (3.27)$$

which will have  $M - 1$  roots or zeros. The orthogonality condition established earlier implies that  $v_i(e^{j\omega})$  will be equal to zero at the complex frequencies present in the signal.

We then form a frequency estimation function as in equation (2).

$$P_{music}(e^{j\omega}) = \frac{1}{\sum_{i=p+1}^M |e^H V_i|^2} \quad (3.28)$$

The unknown frequency components are chosen as the locations of the  $p$  largest peaks in the frequency estimation function of equation 3.28. To demonstrate the resolution capability of MUSIC, a 5 layer profile (with permittivities of 1, 3.4, 3.7, 2.9, 2.7 varying with depth) is considered for example and the radar return signal is modeled using the Plane wave approximation as explained in chapter 2. The SNR of the signal is set to be 0 dB. Figure 3-3 shows the range profiles obtained using the FFT and MUSIC methods.

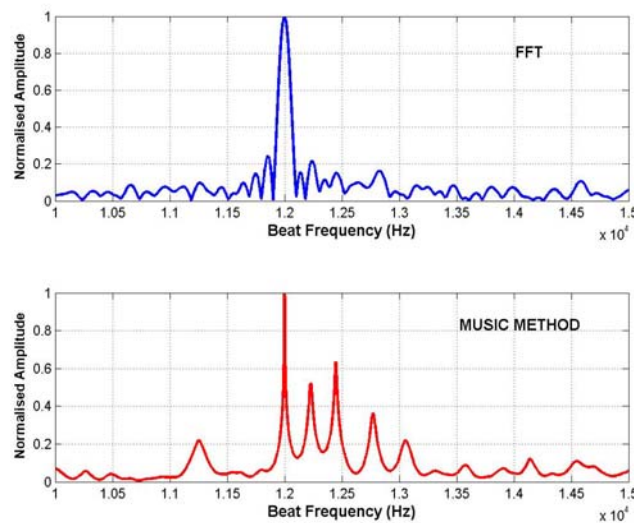


**Figure 3-3 FFT Vs Spectral Estimation Algorithm for enhancement of Profile**

It can be seen that FFT is unable to resolve the reflections due to a very small permittivity contrasts (3.4 to 3.7 & 2.9 to 2.7). The side-lobes of the stronger reflections are clearly masking the weaker returns. The same figure shows the range profile obtained using an algorithm based on spectral estimation, where we find that this technique can effectively be used to enhance weak radar returns.

### **Amplitude Estimation:**

Once the frequency components are chosen, the amplitudes at the location of the peaks can be estimated using the following equation

$$\hat{\mathbf{S}} = \left( \hat{\mathbf{A}}^H \hat{\mathbf{A}} \right)^{-1} \hat{\mathbf{A}}^H \frac{1}{P} \sum_{p=1}^P \mathbf{r}_k^{(p)} \quad (3.29)$$

where  $\hat{\mathbf{A}}$  is the delay parameter matrix which models the sinusoidal base function of a given radar system and  $k = 1, 2, \dots, M$ .  $\hat{\mathbf{S}}$  is a maximum likelihood estimator (for AWGN type noise) and it gives the estimated amplitudes at their corresponding frequencies. Using equations (3.3) and (3.4) recursively, we can estimate the permittivities of each of the layers.

### ***Limitations of Spectral Estimation Based Techniques:***

Spectral estimation techniques for data inversion are very much sensitive to the accuracy of the process model. Any inconsistency in the model can lead to inaccurate estimates of the spectrum and hence, of the model parameters. Also, they do not work well in cases where the Signal to Noise Ratio is too low (say less than 5 dB). As discussed in an earlier section, the fundamental idea in this method is to separate the

signal subspace and the noise subspace. A bad SNR of the signal can distort the decomposed autocorrelation matrix and hence, this method too, is limited in its applications.

There are other eigen vector based methods such as the Minimum Norm Algorithm and the Eigen Vector Method which have subtle differences when compared to the MUSIC algorithm and their performance is close to that of MUSIC.

### **3.4 Summary**

In this chapter, the theory behind two well known methods based on MMSE minimization and spectral estimation were discussed. It was seen that both of these methods can potentially be used for the model parameter estimation problem under a few constraints. In the next chapter, we will look at a few simulations based on these methods and analyze their relative merits and demerits and decide on the approach to be followed when estimating parameters from actual radar data.

# Chapter 4

## Simulations

---

In the previous chapter, various methods for inversion of GPR data were discussed. In this chapter, we present simulations in MATLAB to better understand the working of these methods and to test their performance under various cases. All simulations are done for an Frequency Modulated Continuous Wave (FMCW) radar. The first step is to model the return signal from an FMCW radar.

### 4.1 FMCW Radar Modeling

The FMCW radar transmits a frequency sweep, also called a chirp signal [24] (Figure 4-1). The reflected signal is basically an attenuated and frequency shifted version of the transmit signal.

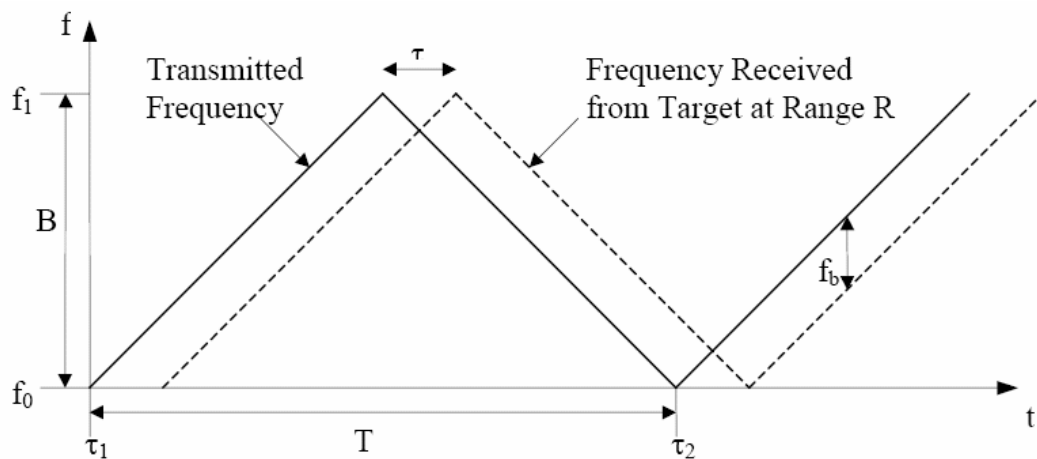


Figure 4-1 FMCW - Chirp Waveform

The composite reflected signal is mixed with a copy of the transmitted signal to determine the range of the target. The difference between the transmitted and the received signal is called the IF Signal or Beat Signal and the shift in received frequency is called the Beat Frequency, which is directly proportional to the range to the target. The instantaneous frequency of the transmit chirp is given by:

$$f(t) = f_0 + \alpha t \quad (4.1)$$

where  $f_0$  is the starting frequency of the chirp,  $\alpha$  is called the chirp rate defined as the ratio of bandwidth ( $B$ ) to the sweep duration ( $T$ ). From the geometry of figure 4-1, we can derive:

$$\frac{\tau}{\left(\frac{T}{2}\right)} = \frac{f_b}{B} \quad (4.2)$$

where  $\tau$  is the two-way time delay experienced by the signal as it strikes the target and returns to the receiver. It can be expressed as:

$$\tau = \frac{2R}{c} \quad (4.3)$$

where  $R$  is the range to the target and  $c$  is the velocity of the EM Wave in free space equal to  $3 \times 10^8$  m/s.

Proceeding further, equation 4.3 can be expanded to yield:

$$f_b = \frac{2RB}{Tc} = \frac{2RBf_m}{c} \quad (4.4)$$

To obtain a mathematical expression for the received signal, let us look at a simple model of the FMCW radar depicted in figure 4-2.

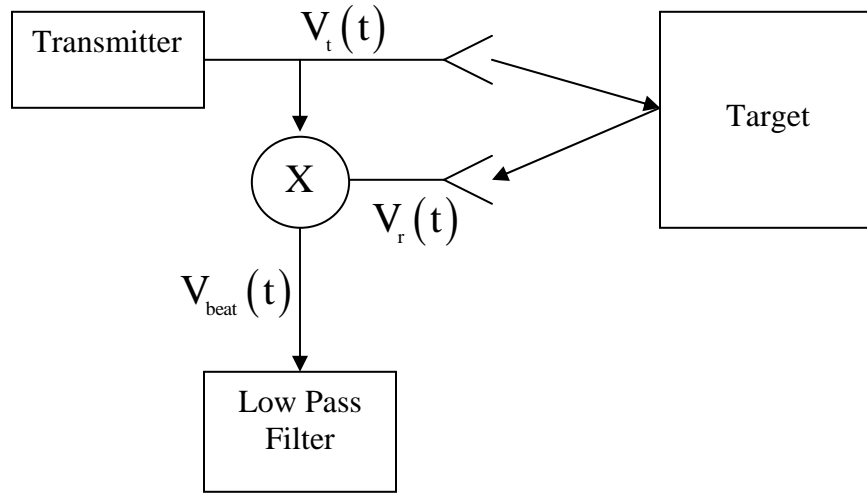


Figure 4-2 Simplified Model of an FMCW Radar

First the transmitted voltage is written as:

$$V_t(t) = A_t \text{Cos}\left(2\pi\left[f_0 t + \alpha t^2\right] + \theta_0\right) \quad (4.5)$$

where  $A_t$  denotes the amplitude of the cosine signal and  $\theta_0$  is the starting phase of the transmitted signal. As discussed earlier, this signal is delayed in time and is also attenuated, by the time it reaches the receiver. Hence, the received signal can be written as:

$$V_r(t) = A_t |\Gamma| \text{Cos}\left(2\pi\left[f_0(t - \tau) + \alpha(t - \tau)^2\right] + \phi\right) \quad (4.6)$$

where  $|\Gamma|$  is the magnitude of the reflection coefficient of a single target and  $\phi$  is the phase of  $\Gamma$ .

This signal reaches the mixer and is mixed with a copy of the transmitted signal  $V_t(t)$ . The output of the mixer consists of two components – the sum and the difference of the two signals. The sum signal, which consists of higher frequency components is filtered using a low pass filter. The output of the low pass filter can be simplified to yield:

$$V_{\text{beat}}(\tau) = |\Gamma| \cos\left(2\pi\left\{f_0\tau + \alpha\tau(2t - \tau)\right\} + \phi_{\text{beat}}\right) \quad (4.7)$$

So far, we have only considered a single target case. Equation 4.7 can be extended to the case where we have multiple target layers. Hence, we need to include the reflection coefficient and delay corresponding to every layer. Also, as seen in chapter 2, the reflection coefficients of subsequent layers depend on the amount of the energy that is transmitted into the previous layers. Hence, the transmission coefficient needs to be included when considering multiple layers. Now, equation 4.7 can be modified to yield:

$$V_{\text{beat}}(\tau) = \sum_{k=0}^{L-1} A_k \Gamma_k \prod_{j=1}^{k-1} T_j \cos\left(2\pi\left\{f_0\tau_k + \alpha\tau_k(2t - \tau_k)\right\}\right) + \mathbf{n} \quad (4.8)$$

All terms carry the same meaning as detailed in chapter 3. As in any radar measurement, we account for noise by modeling it by a Gaussian random variable. Here, we denote this variable as  $\mathbf{n}$ .

The Fast Fourier Transform (FFT) algorithm is applied on the beat signal  $V_{\text{beat}}(\tau)$  to obtain the frequency response of the target, which is also called the Range profile or a plot showing the variation of received amplitude as a function of target distance. The algorithms discussed in the previous chapter will be tested through simulations on an FMCW radar model. All of these simulations were performed using MATLAB.

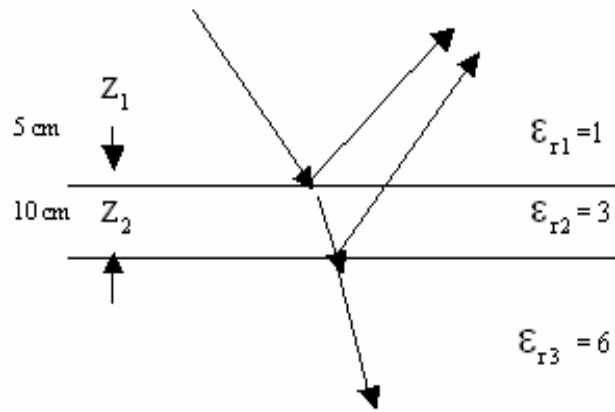


**Figure 4-3 A Multilayered Profile**

To demonstrate the modeling of an FMCW radar, let us assume a multilayered dielectric profile as depicted in figure 4-3 shown above. The test profile consists of three layers with varying permittivity values and corresponding depths. Table 4-1 below shows the parameters considered for simulation along with the geophysical profile vectors  $\epsilon_r$  and  $Z$ .

**Table 4-1 Radar parameters and geophysical parameters for FMCW radar modeling**

Bandwidth	6 GHz
Start Frequency	2 GHz
Sweep time	10 ms
Chirp rate	300 GHz/s
Permittivity vector $\epsilon_r$	[1 3 6]
Depth vector $\mathbf{Z}$ (cm)	[5 10]
Beat frequency vector $f_b = \frac{2RB}{T_c}$ (Hz)	[400 1785.6]

The beat frequencies corresponding to their respective distances are also indicated in the table above. Figure 4-4 below shows the range profile obtained by modeling the above profile of table 4-1 as per equation 4.4.

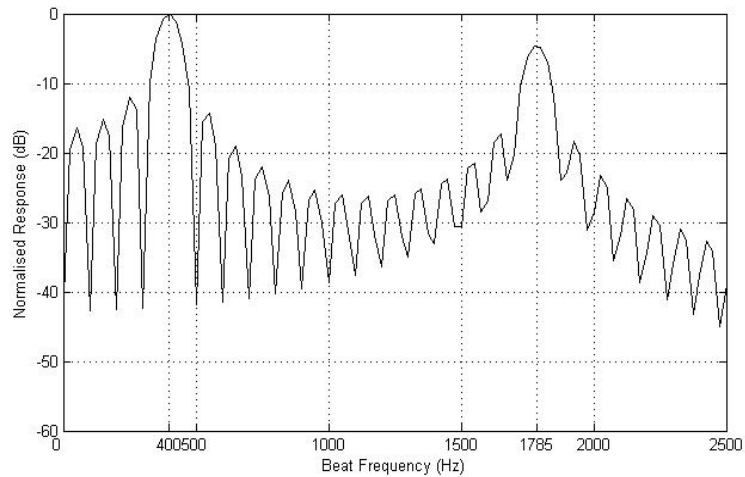


**Figure 4-4 Range Profile obtained by taking IFFT**

We can see peaks corresponding to beat frequencies 400 Hz and 1785.6 Hz which confirms to the mathematically calculated beat frequencies. Now that we have seen the basic principles behind the FMCW radar, we will now look at simulations of three techniques for inversion – The Layer stripping method, Gauss Newton Method and MUSIC Algorithm. At the end of the discussion, we will compare the performance of these methods and decide on the method that can be used for inversion on actual radar data.

## 4.2 Inversion by Layer – Stripping

To illustrate the performance of the layer stripping approach, simulations on an FMCW radar are presented here. Consider a geoprofile along with radar parameters as tabulated in table 4-2.

**Table 4-2 Radar and geophysical parameters to illustrate layer stripping**

Bandwidth	6 GHz
Start Frequency	2 GHz
Sweep time	10 ms
Chirp rate	300 GHz/s
SNR	10 dB
Permittivity vector $\epsilon_r$	[1 1.5 1.9 1.5]
Depth vector $\mathbf{Z}$ (cm)	[8 4 8]

The range profile for this multilayered structure was modeled using MATLAB and is shown in figure 4-5 below.

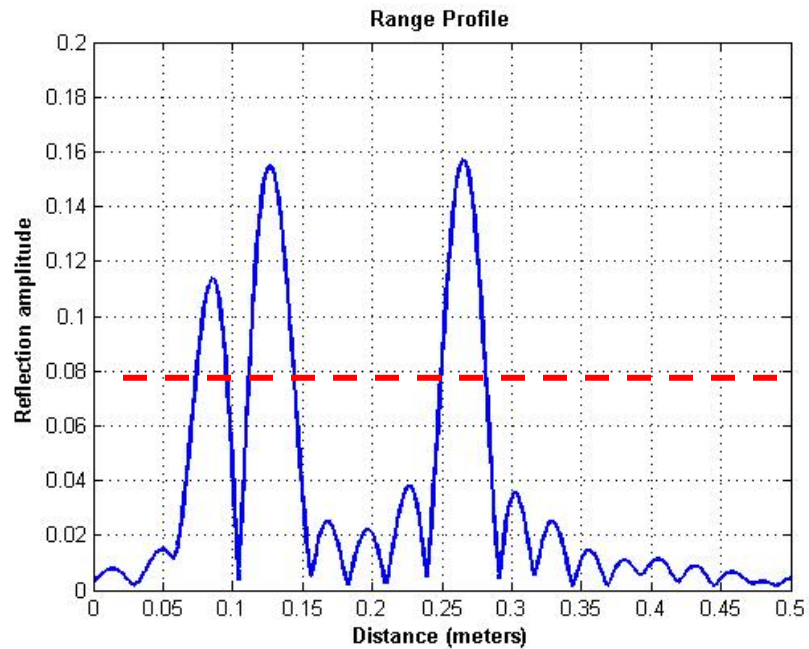


**Figure 4-5 Range Profile obtained using FFT**

From the permittivity vector of table 4-2, there are four dielectric interfaces and hence we see 4 sharp peaks in the figure 4-5. As discussed in Chapter 2, the amplitudes of these peaks correspond to the reflection coefficient of the interface. To estimate the permittivities, we need to set a reasonable threshold. In this case, intuitively, it can be seen that a safe value of 0.07 can be chosen based on the relative amplitudes of signal and noise. (This is indicated by the dashed line in red). Here, it is interesting to note that the interface locations are slightly different from the actual locations. This is because the velocity of the EM wave in every layer is different and it depends on the permittivity of that particular layer. The interface

locations are estimated from the change in slope from negative to positive. From the reflection coefficient values, the permittivities can be calculated by recursively using the formulae (3.3) and (3.4) as discussed in chapter 3. The final reconstructed profile is shown in figure 4-6 below.

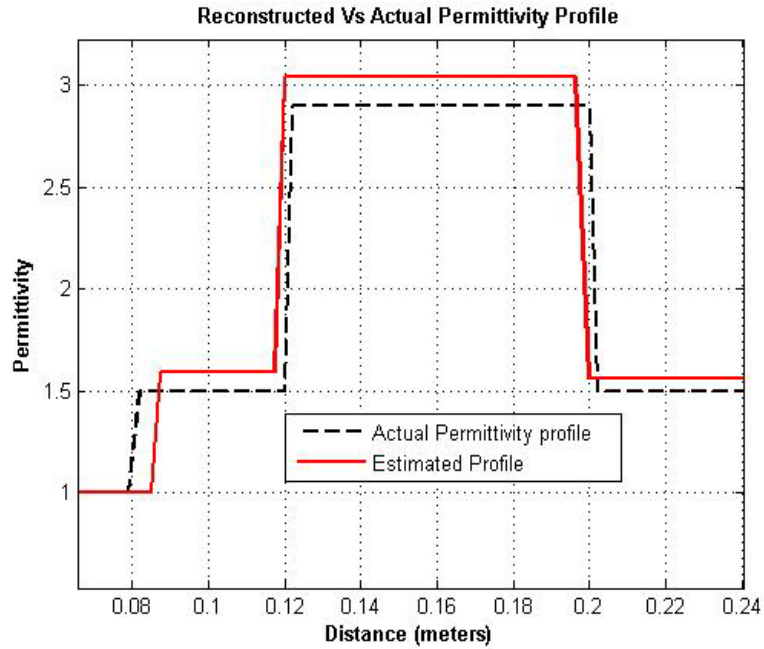


**Figure 4-6 Actual Vs Reconstructed Permittivity Profile**

The importance of setting a reasonable threshold is obvious. To illustrate this, we now consider a profile shown in table 4-3 below to explain the problem of false alarms and missed peaks.

**Table 4-3 Profile chosen to illustrate the problem of false alarms and missed peaks**

Permittivity vector $\epsilon_r$	[1 3 3.5 2 2.8]
Depth vector $\mathbf{Z}$ (cm)	[50 30 40 40]
SNR	5 dB

Figure 4-7 depicts the range profile modeled as in the previous example. As we can see, this data is noisy. The peaks which are checked are valid peaks. To illustrate the problem of missed peaks and false alarms, three thresholds marked as 1,2 and 3 are set as shown in the figure.

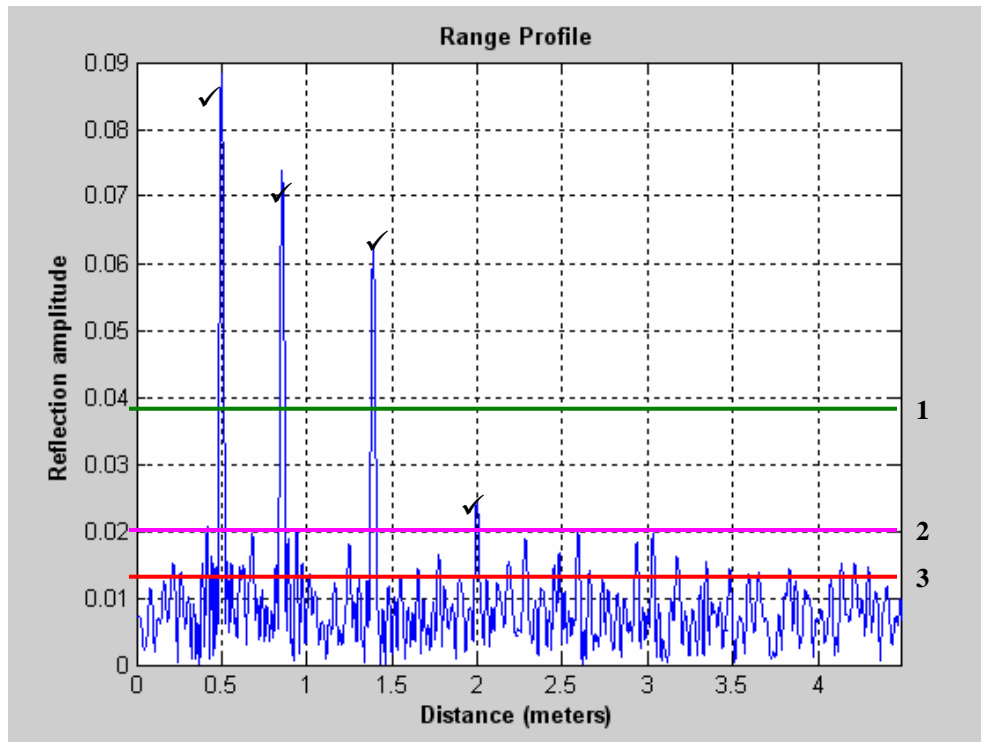


**Figure 4-7 Range Profile of table 4.3 with thresholds marked**

If a threshold corresponding to 1 is set, only the first 3 peaks will be above the threshold and hence we miss the last peak corresponding to the return from the last interface. This is the problem of *Missed peaks* in threshold detection. Hence, the reconstructed profile will not show the last layer.

However, if the threshold is set a value given by 2, all four valid peaks will be detected and we can invert the profile very well. But, if the threshold is set at the value indicated by 3, then several peaks will be detected, apart from the valid peaks. These unwanted peaks are called *False Alarms* and these will result in incorrect permittivity profiles.

#### 4.2.1 The Problem of sidelobes:

In chapter 3, we discussed the problem with FFT's being their inability to resolve closely spaced reflections because of the masking of weak reflections by the sidelobes of the smaller reflections. Since the layer stripping method is based on the range profile obtained using the FFT, the problem discussed above imposes a limitation on the robustness of the method. The following example illustrates this point. Let us consider a profile as tabulated in table 4-4 below and the range profile shown in figure 4-8.

**Table 4-4 Profile chosen to illustrate the problem of sidelobes**

Permittivity vector $\epsilon_r$	[1 3.4 3.7 2.9 3.7]
Depth vector $\mathbf{Z}$ (cm)	[50 8 20 30]
SNR	15 dB

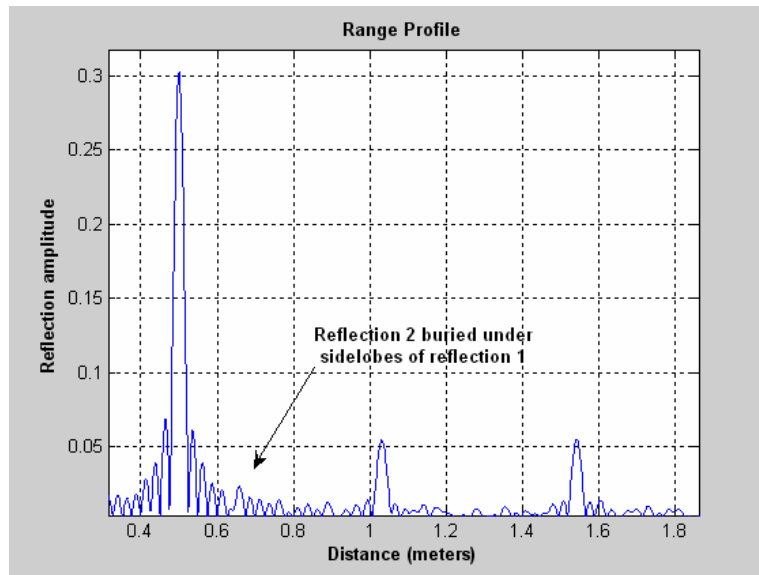


**Figure 4-8 Range profile of table 4-4**

Here we find that, though the SNR of the signal is good, the reflection off the second interface is pretty weak and is hidden under the sidelobes of the reflection from the first layer. Hence, layer stripping fails to detect this buried reflection, and as a result the estimated permittivity profile will look distorted.

Hence, we see that the layer stripping method is useful only when the SNR of the signal is good enough and when the peaks can be sufficiently resolved. Also, it requires the setting of a reasonable threshold value to distinguish between false alarms and valid peaks. This method is also vulnerable to errors because of the problem of sidelobes masking the weak returns. Nevertheless, the layer stripping technique can be used as a first step to get an approximate inverse solution. To overcome the limitations of the layer stripping approach, a few model based techniques were discussed in chapter 3. Let us now look at the performance of the Gauss- Newton method through simulations.

### 4.3 Inversion using Gauss-Newton Method

As discussed in Chapter 3, Gauss Newton method estimates the unknown permittivity profile  $\varepsilon(z)$  by minimizing the difference between the measured and the modeled data. In this section, we will look at a few simulations to perform inversion on modeled FMCW radar data using the Gauss Newton method.

Before we begin to implement the Gauss Newton algorithm, the permittivity model needs to be parameterized. That is, we have to choose basis functions to model the vector of permittivity values. This can be done either by the use of delta functions or B-splines or wavelets as basis functions. B-splines and wavelets provide a smooth variation of permittivity in the model space. However, for the purpose of simple implementation, we decided to use delta functions as basis functions. So, the permittivity model  $\varepsilon(z)$  is parameterized as a vector of delta basis functions i.e.

$$\varepsilon(z) = \varepsilon(z, m) = \sum_{i=1}^N m_i \delta(z - z_i^{(m)}) \quad (4.9)$$

where  $m = [m_1, m_2, \dots, m_N]$  represent the amplitudes of the unknown model parameters (permittivities);  $Z$  represents the depth domain. The delta functions are centered at the knots  $(z_i^{(m)})$  which represents the locations where permittivity changes or locations with dielectric discontinuities. The density of the knot points is dependent on the smoothness of  $\varepsilon(z)$ . This means that, in places where permittivities change rapidly, we might want to space the knots closer than at other places.

### 4.3.1 Example of Parameterization:

Let us consider the profile of table 4.2. Let the radar parameters be so chosen that the resolution of the radar system is 3cm. We need to carefully choose a depth sampling (DS) value such that it fits the discontinuities. The resolution suggests that the radar can resolve targets that are spaced no closer than 3 cm distance. It is generally preferable to choose a DS value that is equal to or less than the range resolution. In this example we find that a DS of 2 cm can successfully locate the dielectric interfaces. Figure 4-9 below illustrates this concept.

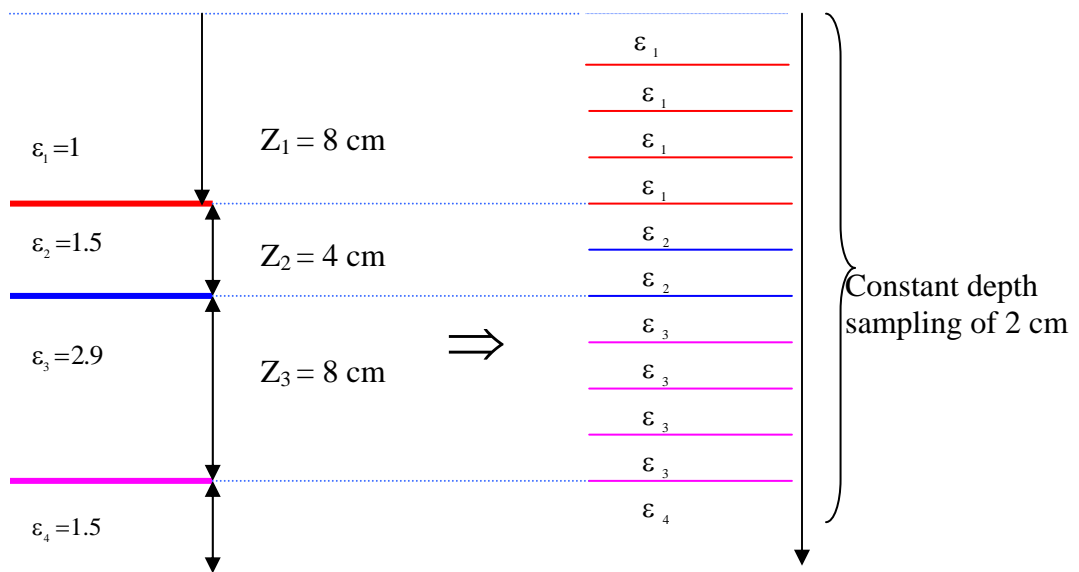


**Figure 4-9 Illustration of parameterization and discretization of depth**

In an ideal case, the finally converged vector of model parameters should read  $\hat{\epsilon} = [1 \ 1 \ 1 \ 1 \ 1.5 \ 1.5 \ 2.9 \ 2.9 \ 2.9 \ 2.9 \ 1.5]$ . Since the DS value has already been set, the above vector can be considered as a set of delta functions with knots equally spaced by DS. Let us now look at the implementation of this

algorithm using MATLAB. Here we present a flowchart (Figure 4-10) that depicts the actual implementation of the Gauss Newton Algorithm.

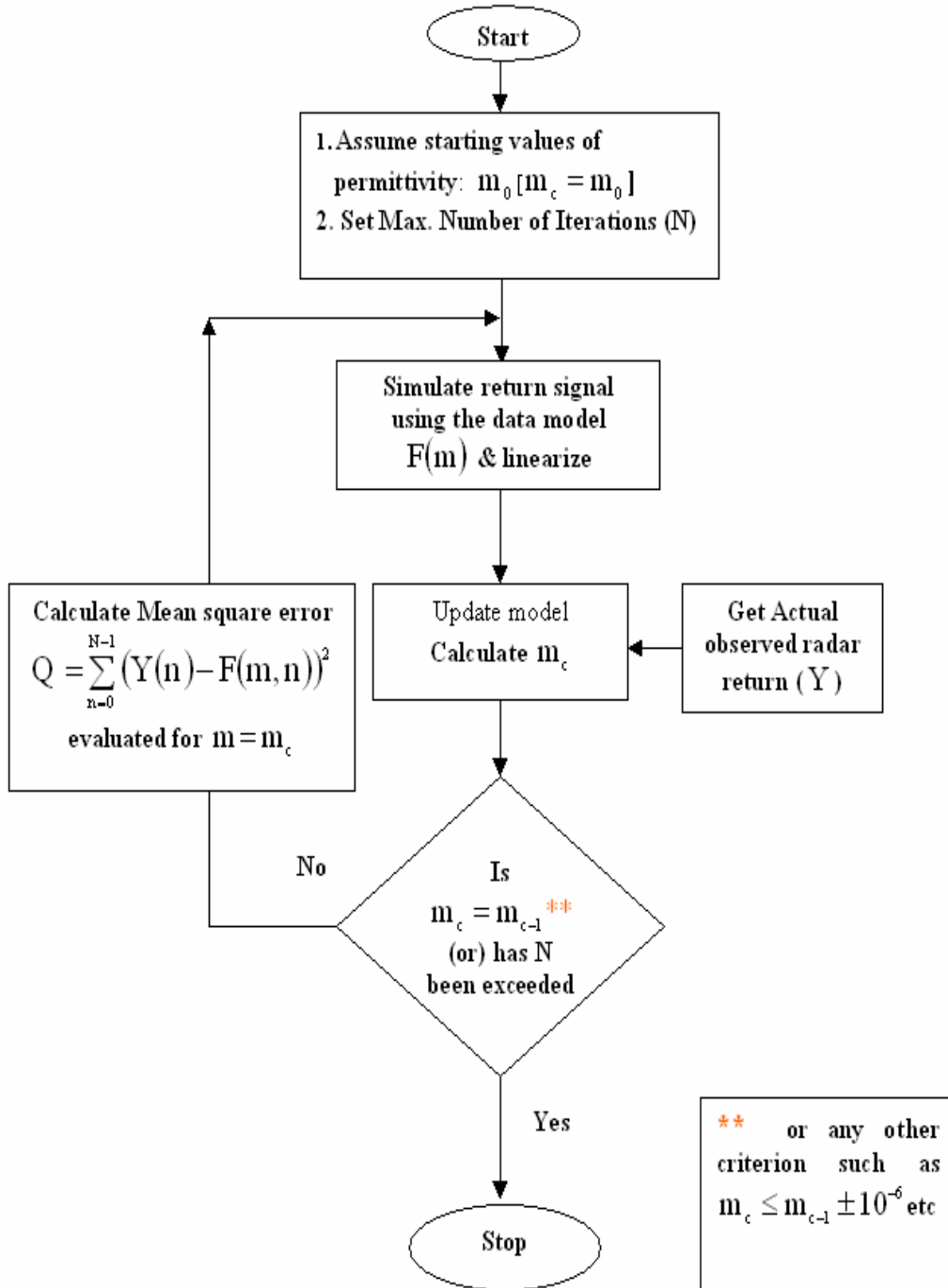


Figure 4-10 Flow chart of the Gauss Newton MMSE estimation algorithm

### 4.3.2 Implementation of the Gauss – Newton Algorithm

To implement this algorithm, we first decide on the number of model parameters to estimate. This is based on apriori information on the approximate depth of the total profile and on the DS value. Once this is set, the algorithm is initiated by a vector of model parameters which are chosen at random, but constrained to lie in an acceptable range of permittivity values. Now, with this set of model parameters, the return signal is modeled using  $F(m)$  and the MMSE criterion of equation 3.5 is evaluated. The next step is to check for convergence, i.e., whether  $m_c = m_{c-1}$ . If this condition is satisfied, convergence is reached and the algorithm can be terminated. If not, the model parameter values are updated as per equation 3.12. During the inversion process using Gauss Newton method, we may have:

1. Local minimum convergence
2. Global minimum convergence
3. No convergence
4. Termination of the algorithm because of ill-conditioned matrix operation

We encountered all of these cases when testing the algorithm for different cases of inversion. The procedure followed in our simulations is to run the algorithm several times (runs) and then pick out the run with the least mean square error.

As depicted in the flowchart, the algorithm is initiated with a starting guess of permittivity values. The number of updating stages for every run (number of iterations) is fixed at some reasonable value (typically 250-1000). The current run is terminated when either of the following conditions are met:

A) Values have converged - This is checked by comparing the current value of the parameters to its previous value, i.e., when

$$m_n = m_{n-1} \quad (4.10)$$

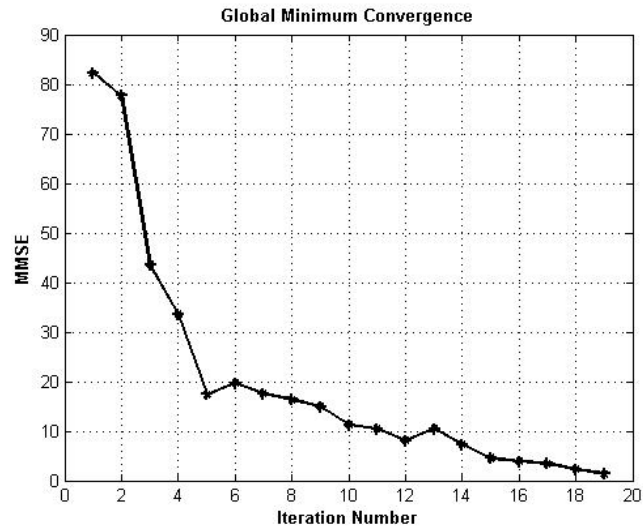
This can mean either a global minimum or a local minimum convergence.

B) Number of iterations exceeds the maximum number of iterations which was set – This means that there is no convergence.

C) Parameter updation enters into a repetitive loop – At this point, the algorithm can be terminated, since it can no longer converge to a global minimum value.

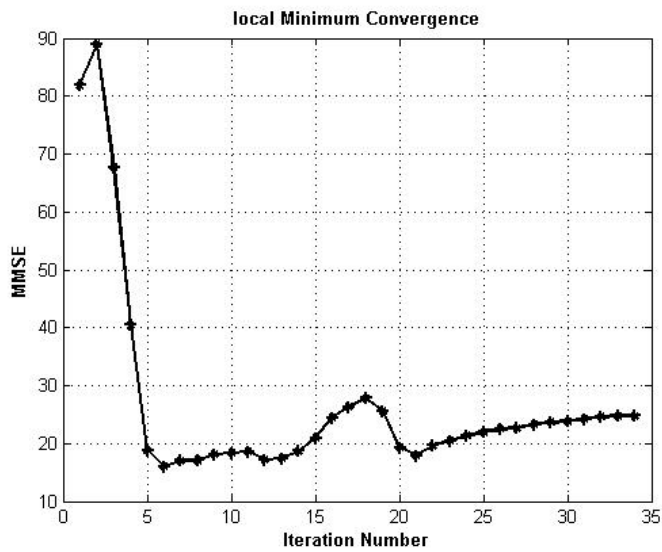
This signals the end of one run. The next run is started with a different starting guess and the same procedure is followed. When all the runs have been completed, the runs that yielded convergence are chosen and their mean square error values are compared to a reference error value, which indicates whether it is a local minimum or a global minimum. The local minimum cases are discarded and the parameter values that yield global minimum are chosen and averaged to yield the final estimate. Figures 4-11 and 4-12 show the MMSE performance for each of the convergence cases discussed so far.

Figure 4-11 below depicts a case of global minimum convergence where the MMSE gradually decreases with every iteration and convergence is reached at the end of 19 runs.



**Figure 4-11 MMSE Vs No. of iterations for Global Minimum convergence**

Figure 4-12 below depicts a case of local minimum. Here, we can see that convergence has been reached after 34 iterations.



**Figure 4-12 MMSE Vs No. of iterations for Local Minimum convergence**

However, the MMSE values do not seem to approach smaller values. At the iteration of convergence, the MMSE value is around 25, which is much greater than the limit set for global minimum. Hence, this is a typical case of local minimum convergence and can be discarded.

Figure 4-13 below shows the error performance of a non-converging case due to the updation falling into a repetitive loop. The MMSE values seem to drop off with every iteration, but soon enter into a never-ending loop. At this point, the current run is terminated and the algorithm proceeds with the next run, starting with a new guess.

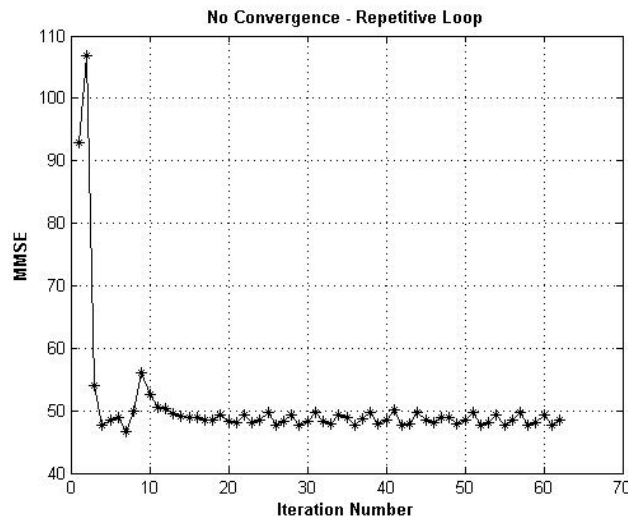
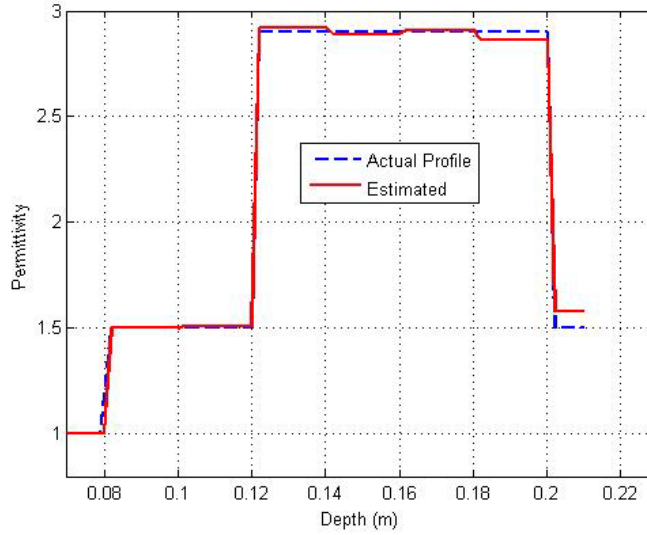


**Figure 4-13 MMSE Vs No. of iterations for No convergence**

In many cases of low SNR, the matrix inversion can become ill-conditioned. Hence, the algorithm will not be able to give any solution.

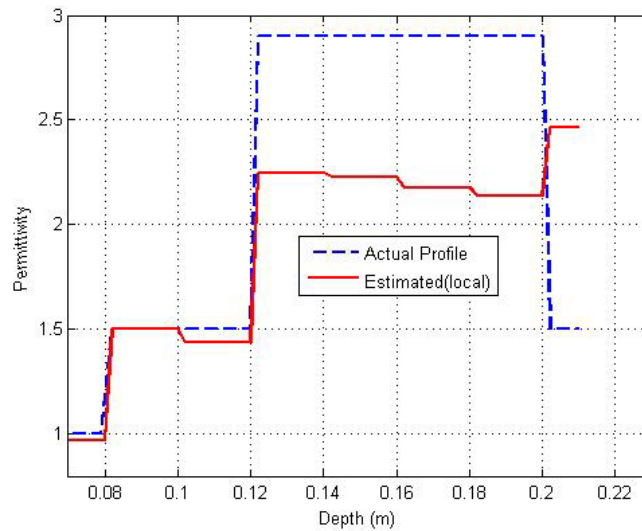
Let us now consider the geo-profile of table 4.2 (with an SNR of 20 dB) to test the Gauss Newton algorithm. For this case, the algorithm was run 20 times with different starting guesses. Here, it was observed that the algorithm converged a total

of 10 times, out of which we could get a global minimum value two times and local minima eight times. The rest were cases of no convergence. The run which gave the least MMSE value has been plotted in the figure below.



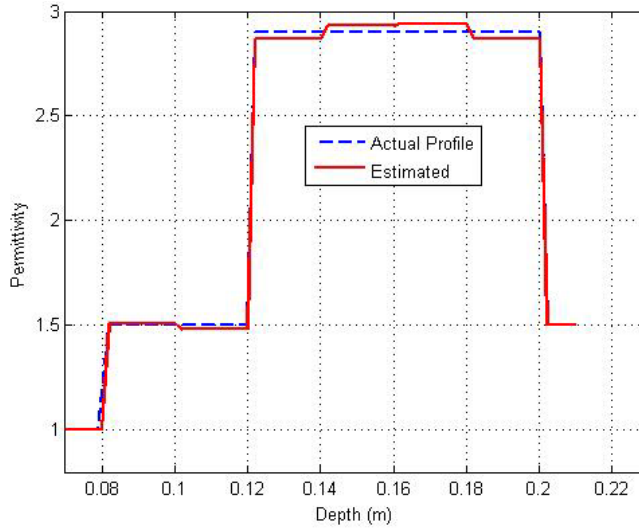
**Figure 4-14 Reconstructed Vs Actual Profile of table 4-2 using Gauss Newton Algorithm**

Figure 4-15 below shows a case of local minimum convergence.



**Figure 4-15 Reconstructed Vs actual profile showing local minimum convergence for profile of table 4-2**

Let us now look at the effect of SNR on the performance of the algorithm. Considering the same profile as in the previous case, but with an SNR of 10 dB, we found that the algorithm yielded a global minimum 4 times out of 50 runs, with the other convergence cases being local minima and many other non-converging cases. Figure 4-16 shows the global minimum convergence result plotted against the actual profile. Here we can observe that the estimated profile is not as close as that for the case of 20 dB SNR.



**Figure 4-16 Reconstructed Vs actual profile for table 4-6 with SNR of 10 dB**

So far, we have only looked at cases where the depths are an integer multiple of DS. In simulations, it might be possible to choose DS values as per the individual depths. However, in practical cases, where we have apriori information about the distribution of the profile, we would want to choose a very small value of DS, say 0.1 cm. We will now pick a case where the depths are not a multiple with DS and analyze the performance of the algorithm. Table 4-5 below shows the profile considered.

**Table 4-5 Geo-profile to illustrate the discretization problem**

Permittivity vector $\epsilon_r$	[1 1.5 2.9 1.5]
Depth vector $\mathbf{Z}$ (cm)	[2 3.31 1.57 ]
SNR	20 dB

Intuitively, we would want to choose a DS of 0.1 cm. That would make all depths a multiple of the DS value. However, with such a small value of DS, the number of model parameters becomes 70. We performed extensive simulations to test the algorithm for estimating a large number of parameters to estimate - typically greater than 15. We found that the algorithm fails to give any useful solution for any number of runs and iterations. Most of the solutions are local minima and there is a large discrepancy between the estimated and the true profiles.

Hence, we decided to choose DS values which are not integer factors of true depths. For this example, choosing a DS of 1 cm does not fit into discontinuities, but we would expect it to yield an approximate profile. However, we found that the solution was spread by a large extent got any number of runs. Hence, this cannot be a reliable solution to our inverse problem. In the next section, we will look at the performance of the MUSIC algorithm, a spectral estimation technique.

## **4.4 Inversion using MUSIC**

Following the theory discussed in chapter 3, we now present a few simulations using the MUSIC algorithm. The input parameters for this algorithm are the radar parameters (such as start frequency, bandwidth, chirp rate, time of sweep,

number of samples), number of snapshots of data, the number of subarrays and number of time delay components (expected).

We will now look at some of the results obtained through simulations. Let us again consider the profile of table 4.2, but with an SNR of 10 dB. As discussed earlier, the first step is the enhancement of the range profile. Figure 4-17 compares the FFT range profile with that obtained using MUSIC after SSP.

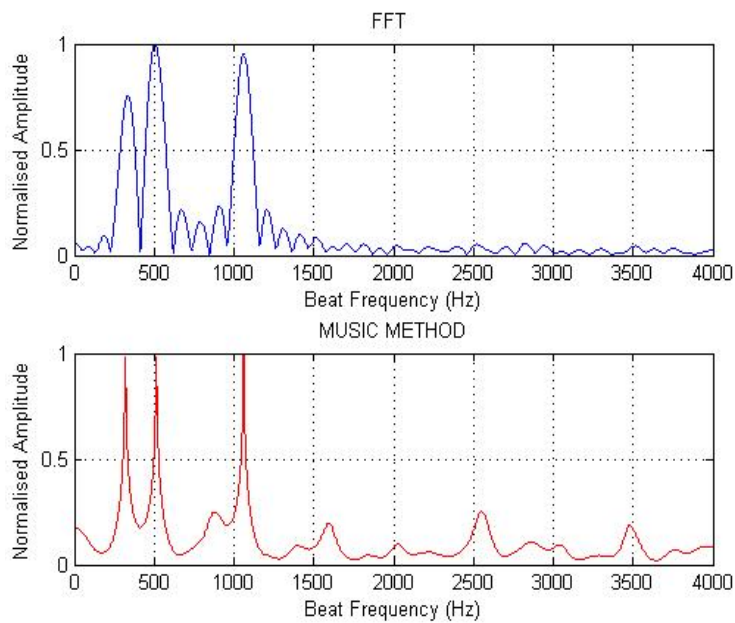


**Figure 4-17 Range profiles obtained using FFT and MUSIC for profile of table 4-2**

It is clearly seen that the resolution is much better using MUSIC where the 3 signal peaks are well defined. From this profile, the corresponding beat frequencies were identified and fed into the amplitude estimation module. The estimated set of parameters match really well with the true parameters and reconstructed profile is plotted in figure 4-18.

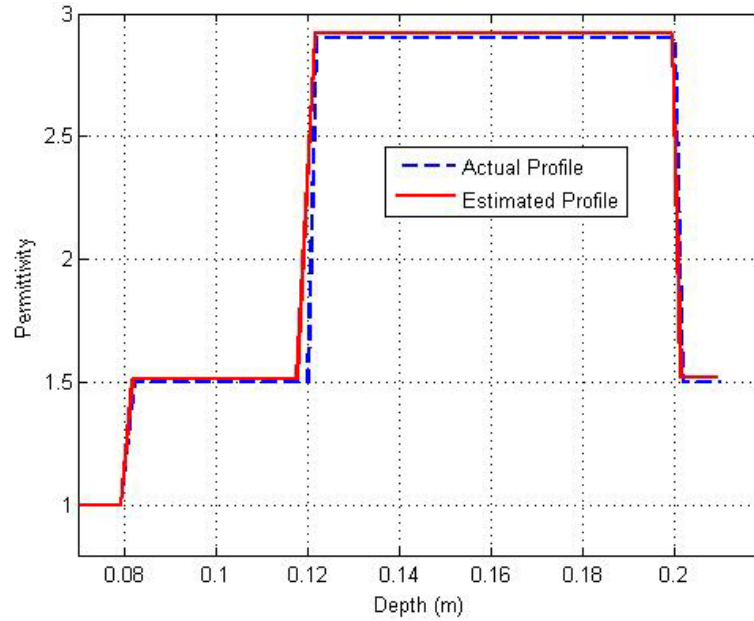


**Figure 4-18 Reconstructed Vs assumed profile of table 4-2 using MUSIC algorithm**

Let us now move on to consider a case where the distances taken at random and are not constrained (Table 4-6) . Also, the SNR in this case is 5 dB.

**Table 4-6 Geo-profile to test MUSIC with random depth profiles**

Permittivity vector $\epsilon_r$	[1 1.5 2.9 1.5]
Depth vector $\mathbf{Z}$ (cm)	[7.3 13.4 87]
SNR	5 dB

Figure 4-19 below compares the range profiles using FFT and MUSIC. After identifying the beat frequencies corresponding to valid peaks, the permittivity profile is reconstructed and is shown in figure 4-20.

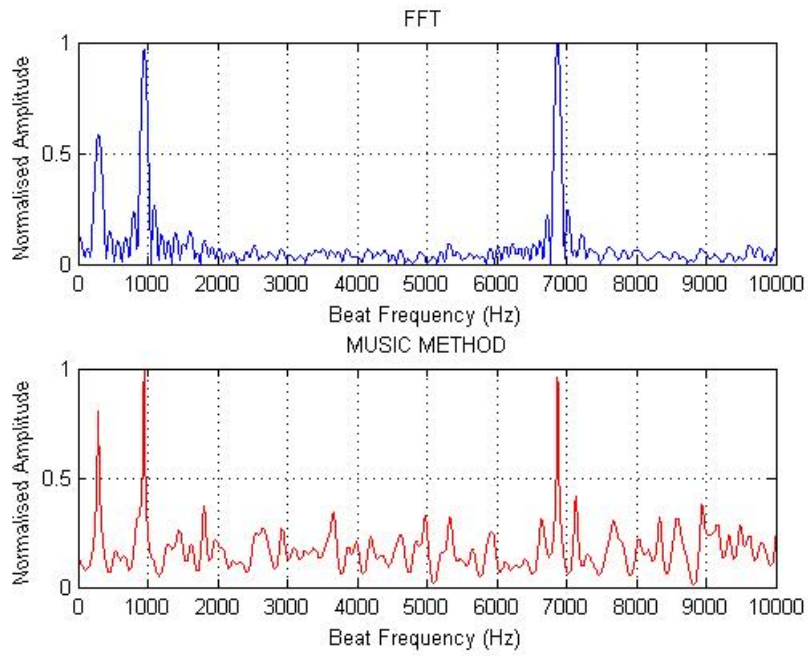


**Figure 4-19 Range Profiles obtained using FFT and MUSIC for profile of table 4-9**

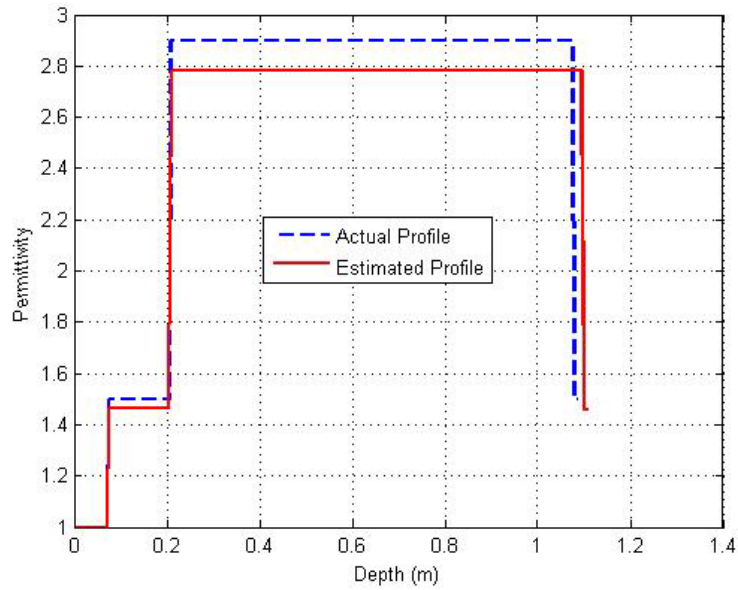


**Figure 4-20 Reconstructed Vs actual permittivity profile of table 4-9**

Hence, we find that MUSIC works well irrespective of the distribution of the depth profile. Next, let us consider a more challenging scenario. Table 4-7 shows an assumed profile.

**Table 4-7 Geo-profile to test MUSIC with the problem of sidelobes**

Permittivity vector $\epsilon_r$	[1 1.5 1.7 1.9 5 3.5 7]
Depth vector $\mathbf{Z}$ (cm)	[13 5 7.5 4 5 4.7]
SNR	10 dB

The range profiles using FFT and MUSIC are compared in figure 4-21 below.

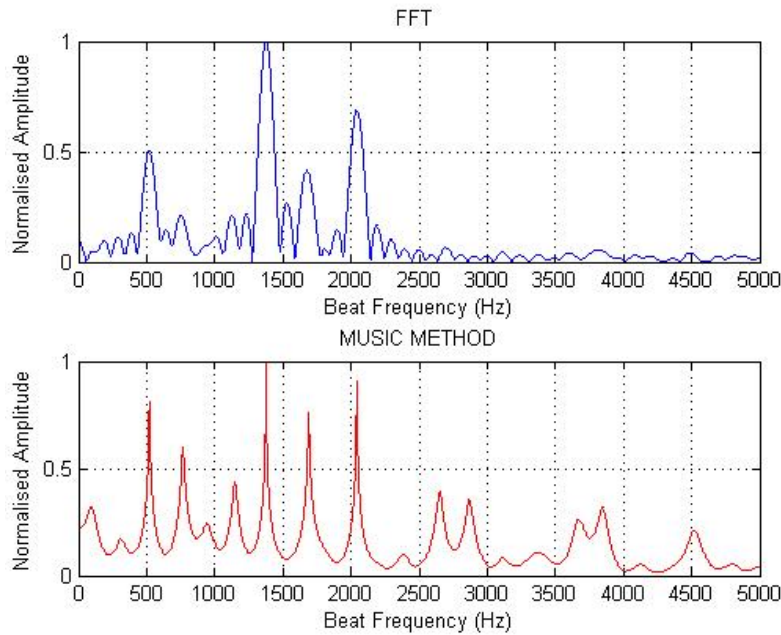


**Figure 4-21 Range Profiles using FFT and MUSIC of table 4-10**

In the FFT profile, we find only four distinctly identifiable peaks due to the sidelobe-masking phenomenon discussed in chapter 3. However, using MUSIC, we

are able to resolve all the valid signal peaks. Figure 4-22 below shows the reconstructed permittivity profile after feeding in the beat frequency values into the estimator.

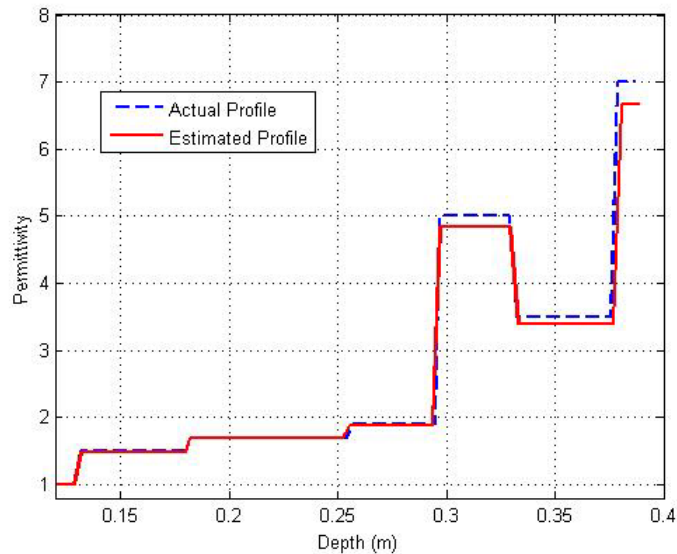


**Figure 4-22 Reconstructed Vs assumed profile of table 4-10**

So far the algorithm has been successful in estimating permittivities in cases of poor SNR and for any distribution of profile – when the right beat frequencies are chosen. To test the robustness of this algorithm, let us now explore what the implications are when:

1. Noise peaks are chosen and
2. Signal peaks are missed

The following test demonstrates this idea. Let us consider the MUSIC-enhanced profile of the earlier example shown in figure 4-23.

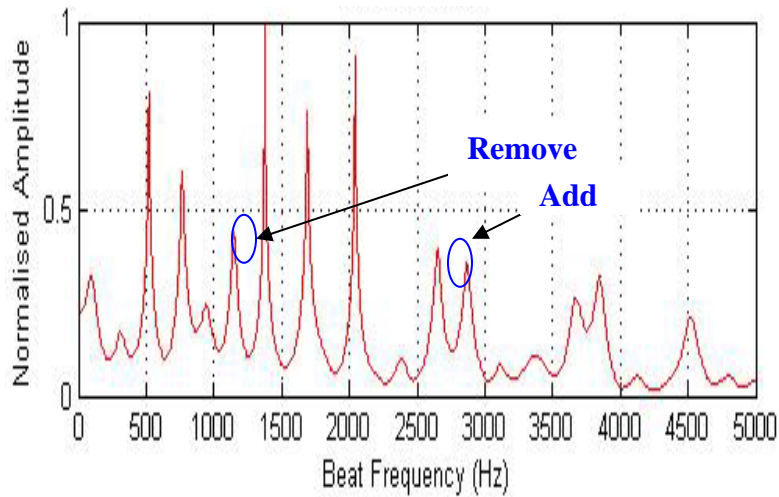


**Figure 4-23 Range profile (using MUSIC) depicting enhancement of weaker reflections**

We shall now make two changes to the beat frequency values fed into the estimator. First, the beat frequency corresponding to 1147.5 Hz will be removed (missed peak) and the beat frequency corresponding to 2654 Hz will be added (False alarm case). Now, with the new set of beat frequency values, we tested the algorithm and the reconstructed profile obtained is shown in the figure 4-24 below.

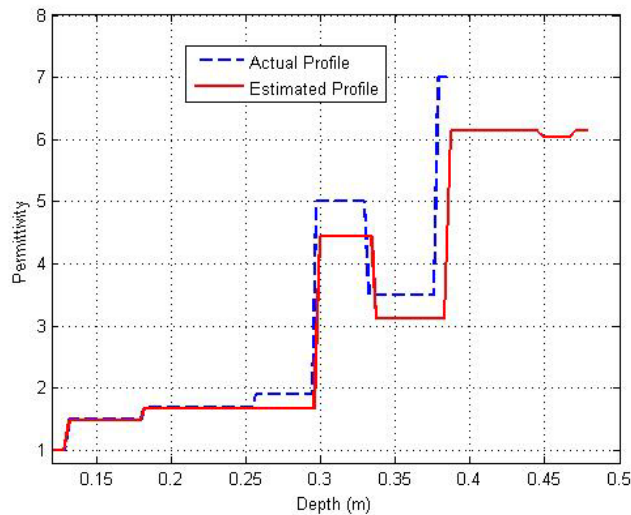


**Figure 4-24 Reconstructed profile obtained after including false alarms in the beat frequency vector**

The reconstructed profile shows that the profile looks slightly distorted, however this error can be tolerated. The selection of false alarms and missed peaks does not drastically alter the reconstructed profile.

## **4.5 Summary**

In this chapter, we analyzed the performance of the layer stripping approach, Gauss Newton method and the MUSIC algorithm for permittivity profile reconstruction. Various cases were considered to test the algorithm for robustness and it was seen that layer stripping works well only under certain conditions; Gauss Newton method is not suitable because it has a few fundamental limitations; whereas MUSIC algorithm performs best even under extreme conditions. In the next chapter, we will apply the MUSIC algorithm to invert actual radar data obtained from field experiments.

# Chapter 5

## Inversion on Actual Data

---

In chapter 4, a few methods for inversion were analyzed through simulations and it was seen that the performance of the MUSIC methods is better than the other methods. In this chapter, we will perform inversion on actual radar data collected from:

1. Field experiments conducted by the Radar Systems and Remote Sensing lab (RSL) in Antarctica during the 2003 field season.
2. Sandbox experiments at the RSL lab.
3. Field experiments conducted by RSL in Greenland during the 2004 field season.

### 5.1 Experiments in Antarctica

The RSL at the University of Kansas used an Ultra Wide-Band (UWB) Frequency Modulated Continuous Wave (FMCW) radar to determine snow thickness over sea-ice. We will use data collected during the 2003 field season in Antarctica to validate the working of the inversion algorithm. The estimated permittivity profiles will be compared with profiles obtained from in-situ snow-pit measurements. A model of the snow radar system and the dielectric structure of the test site as given in

[25] is depicted in figure 5-1. The parameters of the UWB radar are tabulated in table 5-1.

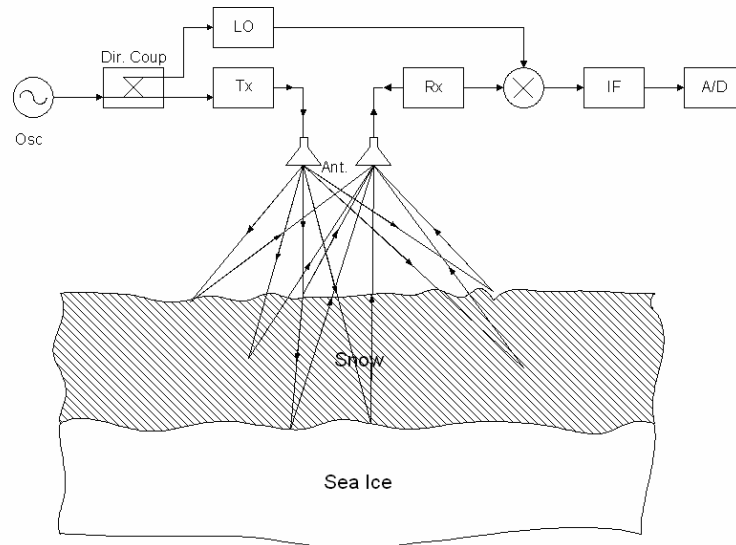


**Figure 5-1 Model of the Snow radar used in Antarctica.**

**Table 5-1 Parameters of UWB FMCW radar used in Antarctica**

Characteristic	Value	Unit
Radar Type	FM-CW	
Sweep Frequency	2-8	GHz
Range Resolution	$\cong 4$	cm
Sweep Time	10	msec
Transmit Power	13	dBm
PRF	25	Hz
Sampling Rate	5	MHz
Antenna	TEM Horn Antenna	

It can be seen that the dielectric structure consists of a layer of air, followed by several layers of snow and a homogeneous layer of sea ice extending all the way upto the bedrock. Air is modeled with a permittivity of one. Sea ice can be modeled using the Tinga mixing model given in [9]. However, for simplicity, the permittivity of sea ice can be taken to be approximately 3.14 in the microwave frequency region. Modeling the permittivity of snow requires parameters such as density, wetness and other factors which can be obtained from snow-pit measurements. From these parameters, the complex permittivities can be calculated using appropriate mixing models from literature [9]. Table 5-2 shows the in-situ measurements taken at one of the test sites in Antarctica where the FMCW radar was tested. The models used to calculate the permittivities are presented in the next section.

**Table 5-2 Snow pit measurements**

<b>Layer Thickness (m)</b>	<b>Density (g/cm<sup>3</sup>)</b>	<b>Salinity [‰]</b>	<b>Wetness [Vol %]</b>
1.83	1.40	0	0
0.03	0.191	0.145	-0.46
0.03	0.254	-	0.73
0.03	0.328	0.07	0.09
0.03	0.364	0.31	0.00
0.03	0.355	0.11	0.00
0.03	0.334	0.21	0.00
0.03	0.285	0.20	0.39
0.03	0.293	0.12	0.49
0.03	0.244	0.31	1.41
0.03	0.254	0.34	1.67
0.03	0.245	0.30	1.76
0.03	0.226	0.27	1.96
0.03	0.309	0.05	0.31
0.03	-	2.17	3.00
0.015	-	29.4	3.28

### 5.1.1 Modeling the complex dielectric constant of snow cover on sea-ice

Snow can typically occur in two phases – dry and wet. Dry snow is a mixture of ice and air and does not contain water, whereas wet snow includes water. Table 5-2 shows that the Antarctic snow is a mixture of wet snow and brine.

To model the dielectric constant of this mixture, we first model the permittivity of wet snow using the empirical *Debye-like model* [9], where the real part of permittivity is mathematically modeled as:

$$\epsilon'_{ws} = A + \frac{B m_v^x}{1 + \left(\frac{f}{f_0}\right)^2} \quad (5.1)$$

and the imaginary part is modeled as

$$\epsilon''_{ws} = \frac{c \left(\frac{f}{f_0}\right) m_v^x}{1 + \left(\frac{f}{f_0}\right)^2} \quad (5.2)$$

where  $f_0 = 9.07 \text{ GHz}$ , the effective relaxation frequency of wet snow,  $m_v$  denotes the Moisture content in volume percentage,  $c$  represents the free space velocity,  $f$  is the frequency variable and the constants  $A$ ,  $B$  and  $x$  are derived from experimental data as given in [9]. Once the wet snow permittivity has been modeled, we then model the permittivity of brine using the formulation developed by Stogryn [26]. The real and imaginary parts of the complex dielectric constant of brine are given as:

$$\epsilon'_b = \epsilon_{w\infty} + \frac{\epsilon_{b0} - \epsilon_{w\infty}}{1 + (2\pi f \tau_b)^2} \quad (5.3)$$

$$\epsilon_b'' = \frac{2\pi f \tau_b (\epsilon_{b0} - \epsilon_{w\infty})}{1 + (2\pi f \tau_b)^2} + \frac{\sigma_b}{2\pi \epsilon_0 f} \quad (5.4)$$

where  $\epsilon_{w\infty}$  is a dimensionless quantity equal to the high frequency limit of the dielectric constant of pure water,  $\epsilon_{b0}$  is the static dielectric constant of brine,  $\sigma_b$ ,  $\tau_b$  are the conductivity and relaxation time respectively of brine and are empirically related [9] to the normality and temperature of brine in the mixture.

Finally, we model the permittivity of the mixture by treating brine as an inclusion within a wet snow mixture and using the mixing formula as given in [27].

$$\Delta\epsilon_{\text{mix}} = \frac{\chi V_b \{ \epsilon_b - \epsilon_{ws} \}}{\left[ 1 + \left( \frac{\epsilon_b}{\epsilon_{ws}} - 1 \right) A_0 \right]} \quad (5.5)$$

From equation 5.5, the effective permittivity of the mixture is calculated as

$$\epsilon_{\text{eff}} = \epsilon_{ws} + \Delta\epsilon_{\text{mix}} \quad (5.6)$$

where  $\epsilon_{ws} = \epsilon'_{ws} + j\epsilon''_{ws}$ , the complex permittivity of wet snow,  $\chi$  denotes the coupling factor considering brine inclusions to be isotropically oriented oblate spheroids,  $A_0$  is the depolarization factor and  $V_b$  is the brine volume fraction which is a function of the salinity and temperature of brine [9].

Evaluating the above expressions, the effective permittivities and their corresponding distances are tabulated in table 5-3 below.

**Table 5-3 Modeled Permittivity Profile**

Layer Thickness (m)	$\epsilon_{effective}$ (Modeled - complex)	$\epsilon_{effective}$ (Modeled - Absolute)
1.83	1.00	1.00
0.03	1.45+j0.0193	1.44
0.03	1.60 + j 0.0175	1.60
0.03	1.70 + j 0.0021	1.70
0.03	1.77 + j 0.0044	1.77
0.03	1.74 + j 0.0016	1.74
0.03	1.71 + j 0.0029	1.71
0.03	1.64 + j 0.0104	1.65
0.03	1.66 + j 0.0121	1.66
0.03	1.66 + j 0.0462	1.67
0.03	1.71 + j 0.0576	1.71
0.03	1.70 + j 0.061	1.71
0.03	1.69 + j 0.0692	1.69
0.03	1.67 + j 0.0066	1.68
0.03	2.19 + j 0.1739	2.20
0.015	6.13 + j 1.2496	6.35
Ice bottom	3.14	3.14

The permittivity profile of table 5-3 is plotted in figure 5-2.

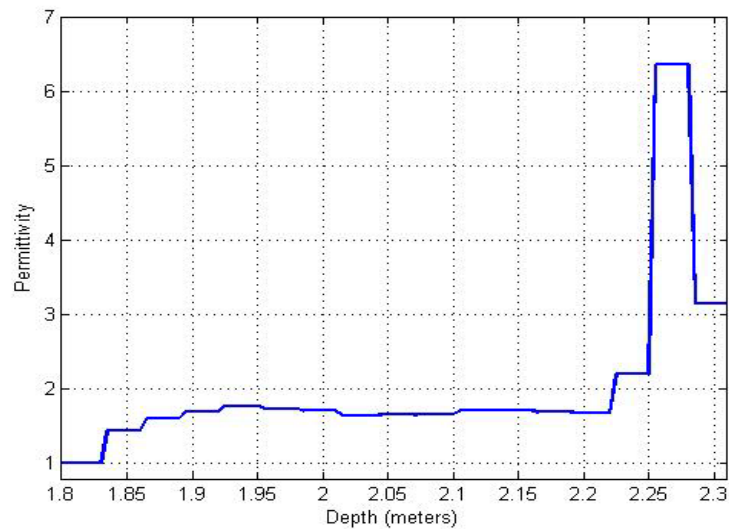


**Figure 5-2 Permittivity profile of table 5-3**

We now apply the inversion algorithm on actual radar measured at the same site. Figure 5-3 below shows the echogram of the test site. The core data that was modeled earlier corresponds to A scopes 1-40.

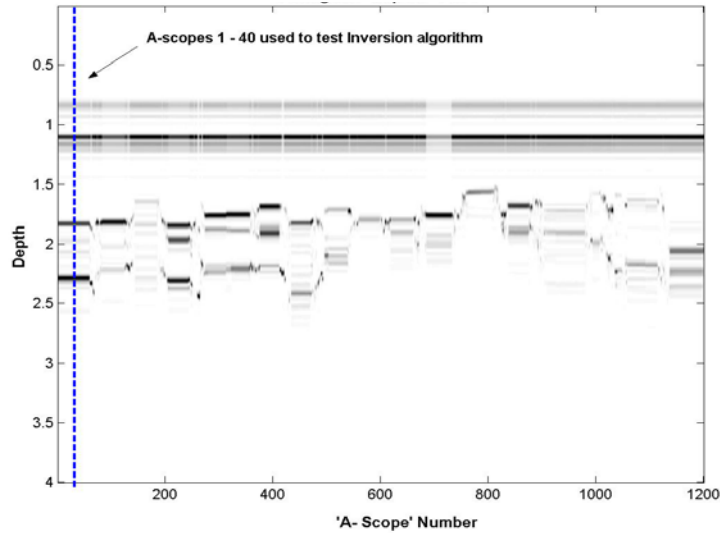


**Figure 5-3 A-scope of radar measurements**

Any of the A scopes between 1 and 40 can be chosen for inversion. Let us choose A-scope 20. Figure 5-4 below shows the range profile of A-scope 20 plotted using FFT.

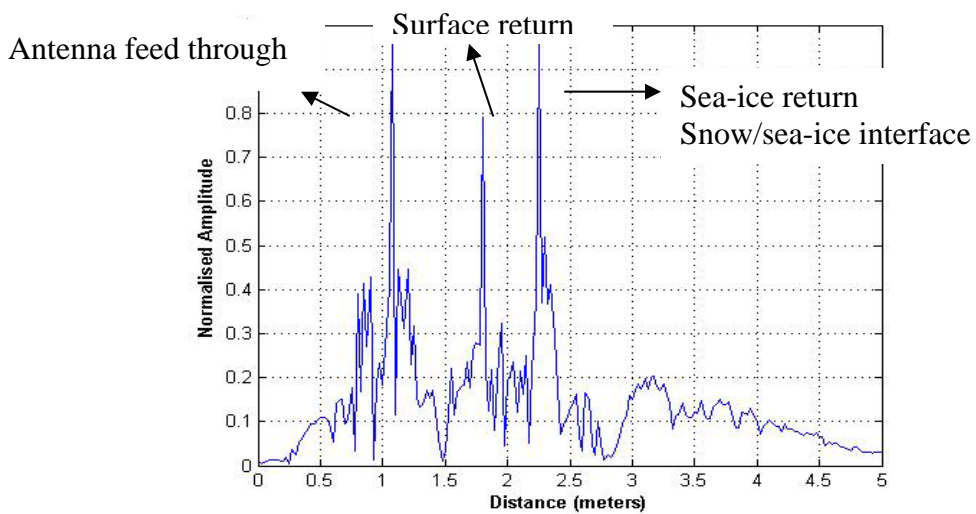


**Figure 5-4 Range Profile plot of A-scope 20**

From figure 5-4, we can see three well defined peaks corresponding to

1. Antenna feed through return
2. Return from surface layer (Air/Snow interface) and
3. Return from snow/sea-ice interface

Apart from these peaks, there are other smaller peaks which correspond to internal snow layers. Before applying the inversion algorithm, the first step is to remove the radar system effects and the antenna feed-through using calibration data. A flat metal screen is used as the target and the return signal is collected and the main peak (corresponding to the plate) is filtered out. The filtered signal now represents the impulse response of the system and is commonly used to account for system effects (which also includes the antenna response).

The Fourier transform of this signal gives the transfer function of the radar system  $X(f)$  and can be eliminated from the observed return  $Y(f)$  using equation 5.7 to yield the response of the target  $\Gamma(f)$ .

$$\Gamma(f) = \frac{Y(f)}{X(f)} \quad (5.7)$$

The next step is to remove the antenna feed through by using a band-pass filter. The range profile after calibration and filtering is shown in figure 5-5 below. Now, the data can be fed into the inversion algorithm. Clearly, the reflections from internal snow layers need to be resolved.

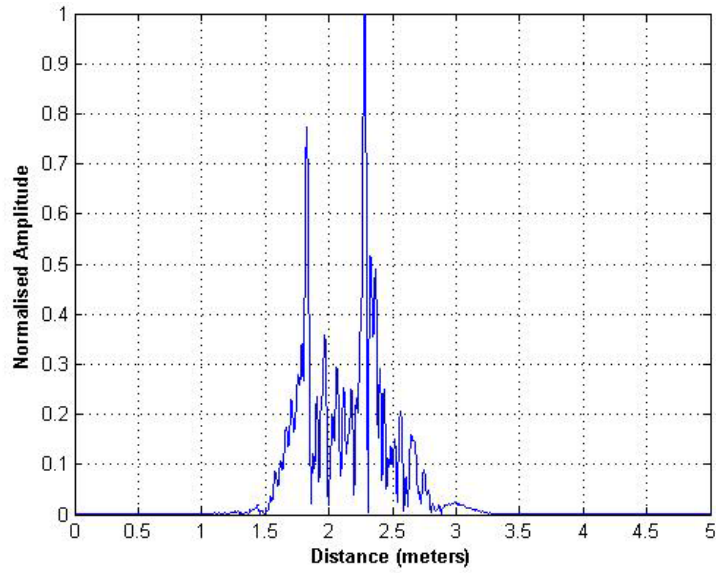


**Figure 5-5 Range Profile after calibration and filtering**

As seen in chapter 4, we first apply MUSIC on this data and enhance the spectrum.

Figure 5-6 below compares the range profiles obtained using FFT and MUSIC.

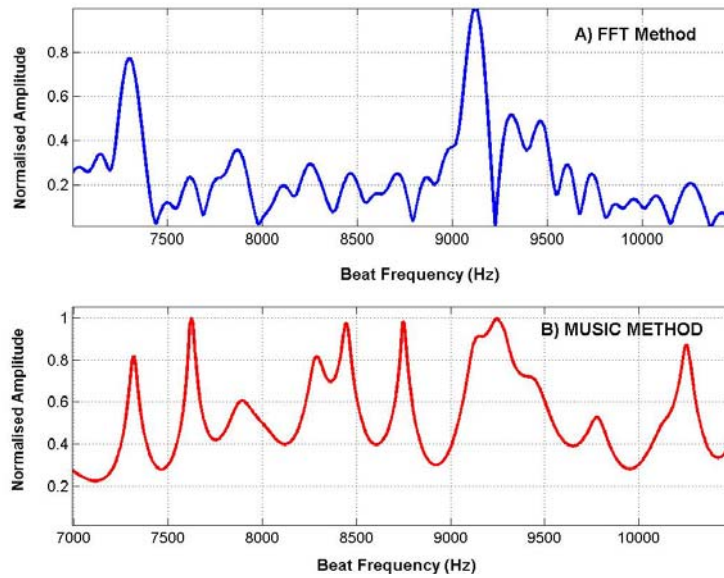


**Figure 5-6 Range Profiles obtained using FFT and MUSIC**

The beat frequencies detected from the enhanced range profile are tabulated in table 5-4 below.

**Table 5-4 Comparison of estimated beat frequencies of core with those of FFT and MUSIC**

Beat Freq $F_B$ (Core data) Hz	Beat Freq $F_B$ (MUSIC) Hz	Beat Freq $F_B$ (IFFT) Hz
7320	7317.0	7290
7474	7622.0	7860
7630	7885.0	9120
7781	8290.0	
7936	8445.0	
8088	8748.5	
8243	9150.0	
8399	9240.0	
8559	9770.0	
8721		
8884		
9047		
9203		
9390		

These beat frequency values were fed into the estimator and the reflection coefficients were estimated. These values were then used to estimate the corresponding layer permittivities by using equations 2.1 and 2.2 recursively. The estimated permittivity profile is plotted against the actual profile (modeled) in figure 5-7 below.

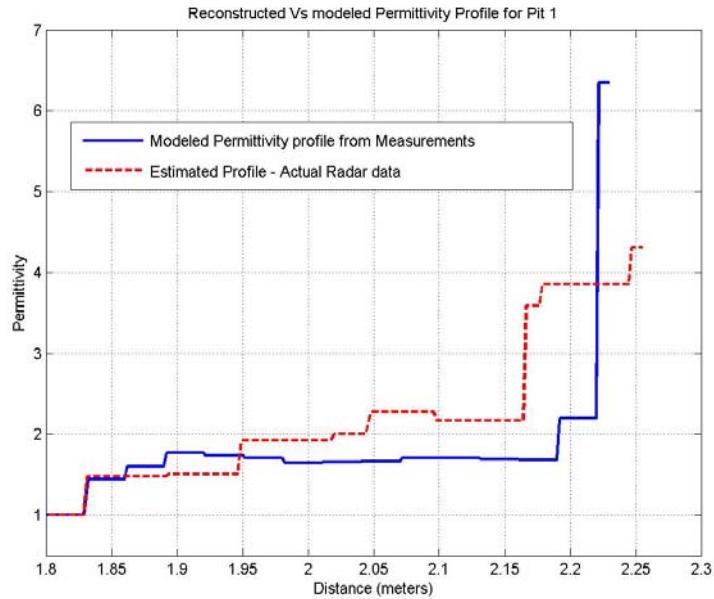


**Figure 5-7 Reconstructed Vs modeled profile for Pit 1**

It can be seen from the above profile that the MUSIC-estimated profile matches reasonably well up to a certain depth, but gradually deviates from the measured values, as we move into deeper layers. This deviation is expected, because, at depths closer to the snow pit, the signal is greatly attenuated because of significant salinity as shown in column 3 of Table 5-2, which was not factored in the reconstruction of the permittivity profile.

Other variations in the estimated profile could be attributed to: (1) a discrepancy in the model representing the radar return, (2) an error in calibration data, (3) very subtle changes in the permittivity that MUSIC is not able to distinguish, and (4) measurement errors in the field that cannot be compensated for at this stage, since we are using an existing data.

The algorithm was also tested at two other locations where measurements were made using the same FMCW radar. Figure 5-8 shows the range profiles using FFT and MUSIC on data measured at one of the pits (Pit 2) on September 28, 2003.

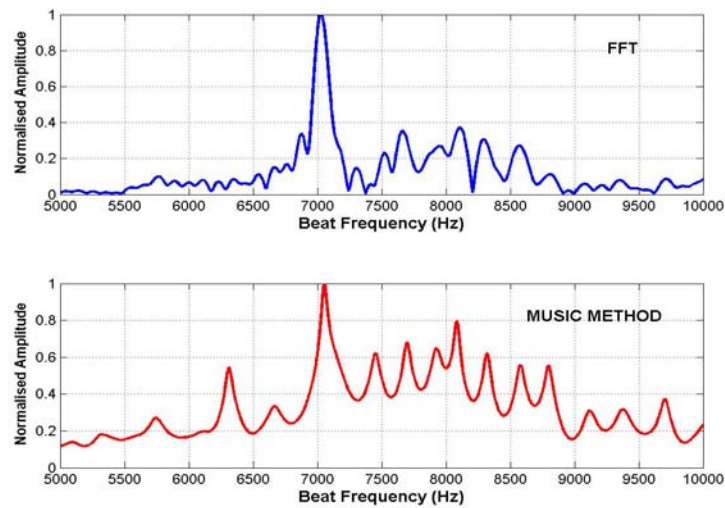


**Figure 5-8 Range Profiles obtained using FFT and MUSIC for Pit 2**

Following the same procedure, the reflection coefficients were estimated and the reconstructed permittivity profile is plotted in figure 5-9 below.

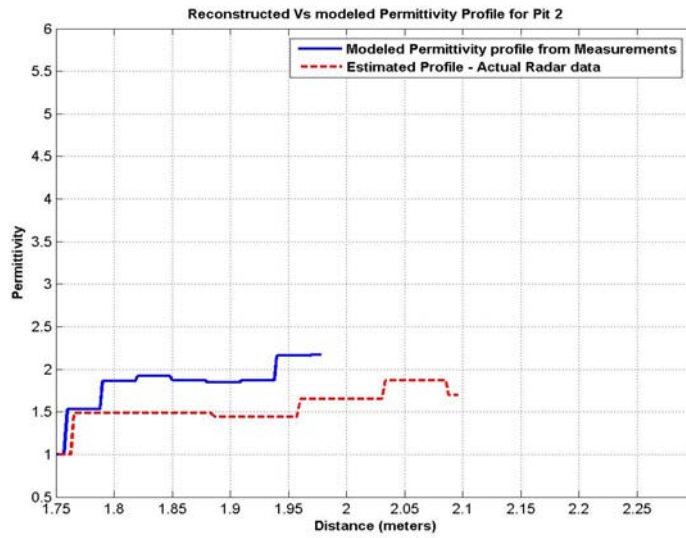


**Figure 5-9 Reconstructed Vs modeled profile for Pit 2**

Similarly, the algorithm was also tested on another location on October 14 (Pit 3). The range profiles and the reconstructed permittivity profiles are depicted in figures 5-10 and 5-11 respectively.

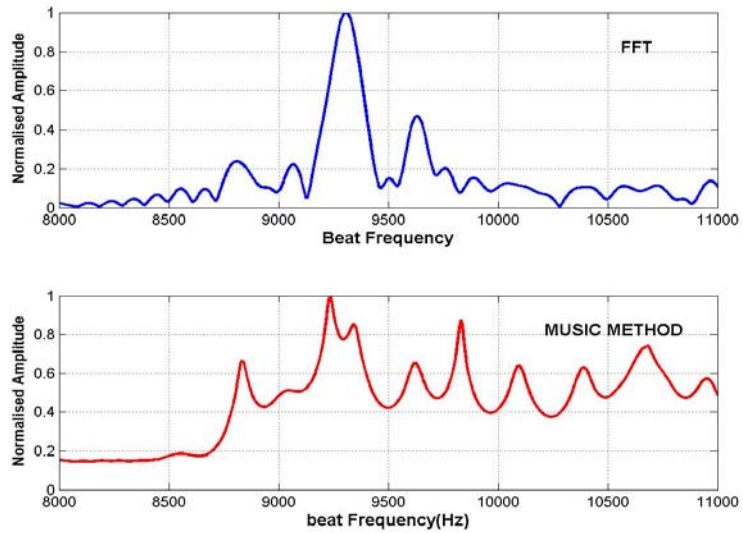


**Figure 5-10 Range Profiles obtained using FFT and MUSIC for Pit 3**

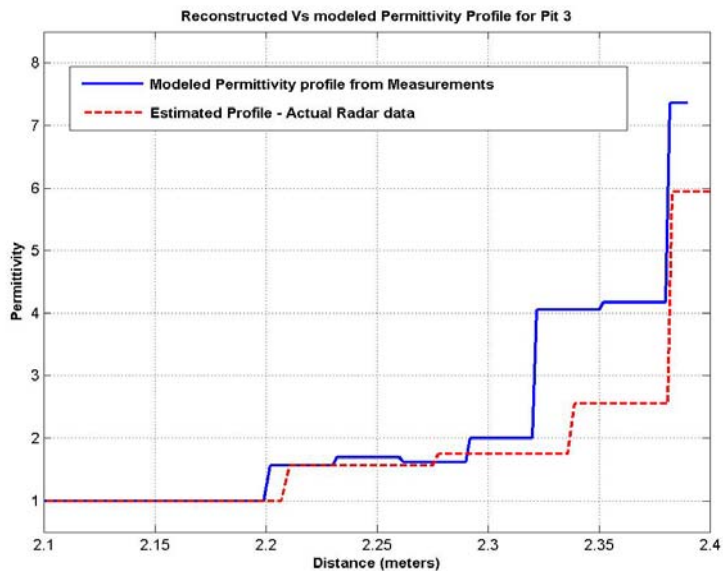


Figure 5-11 Reconstructed Vs modeled profile for Pit 3

## 5.2 Tests at the Sandbox lab at RSL

The inversion algorithm was also tested in the sandbox facility of the RSL lab at the University of Kansas. This facility consists of a rectangular box filled with quartz sand and is built with a system such that an antenna can be mounted to be looking downwards (towards the sand). A network analyzer is used in place of a radar and is connected to the antennas using RF cables. The network analyzer is connected to a computer using a General Purpose Interface Bus (GPIB) card and can be controlled using MATLAB. A detailed description of the sandbox set-up and the RF circuitry is given in [28].

The operating parameters such as start frequency, bandwidth, number of samples and sweep time are set in the network analyzer and calibration is performed at the input to the antennas. To remove system effects, a flat aluminium plate is laid

over the sand surface and  $S_{11}$  measurements are taken. Then the targets are buried under sand and the  $S_{11}$  is measured over the frequencies of interest. Typically, the mismatch between the cable and the antenna is very large and its sidelobes can mask small reflections buried under sand. This mismatch is removed by performing a sky test where the antenna is pointed upward in such a way that there is no reflecting surface atleast within the maximum unambiguous range of the system. The sky test measurements are then subtracted from the actual measurements and the Fourier transform of this signal yields the range profile.

The inversion algorithm was tested by using a HP 8753D network analyzer. The network analyzer parameters are tabulated in table 5-5 below. A TEM horn antenna (operating in the 2-18 GHz frequency range) was used to take measurements. A bandwidth of 5 GHz was chosen so that we could have a resolution of 3 cm. Such a fine resolution is desired so that we could stack up layers (wood, Styrofoam) of small thickness in such a way that the measurements could be taken would altering the antenna arrangements in the sandbox.

**Table 5-5 Network Analyzer Parameters for Sandbox experiment**

Start Frequency	2 GHz
Stop Frequency	7 GHz
Number of frequency samples	1601
Sweep time	800 ms
Transmit Power	0 dBm
Calibration type	1 port
IF Bandwidth	3000 Hz
Antenna type	TEM Horn
Antenna Gain	10 dB

The network analyzer was set in the stepped frequency mode so that it is equivalent to a stepped-frequency radar. As described earlier, the network analyzer was interfaced with a computer and single port calibration was performed. Then, the sky shot measurements were taken. Figure 5-12 shows the target structure that was set-up to test the inversion algorithm.

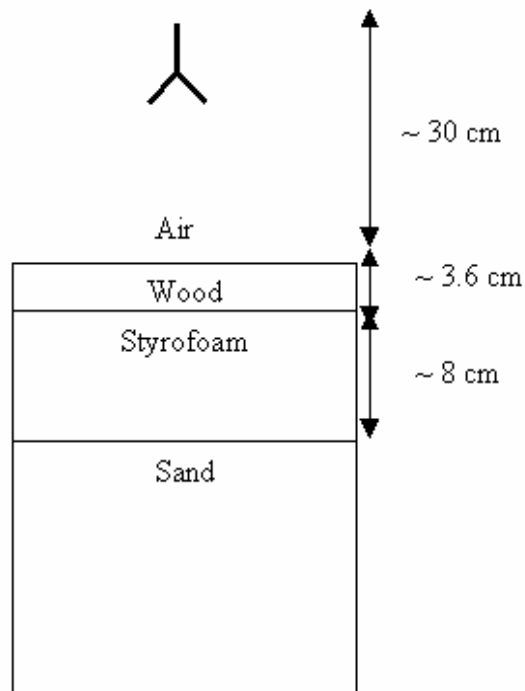


**Figure 5-12 Multilayered Target stack to test inversion algorithm**

It can be seen that there are four layers which form a dielectric stack giving rise to three interfaces. Figure 5-13 below shows the average of 50 sky shot measurements taken to remove the antenna-cable mismatch.

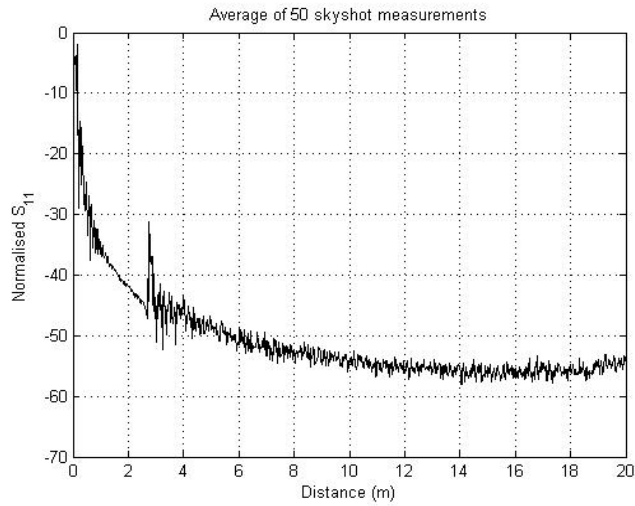


**Figure 5-13 Average of 50 sky shot measurements**

Next, measurements were taken after placing a flat Aluminium plate over the surface of sand. The measured return is plotted in figure 5-14 and is subtracted from the skyshot signal (figure 5-15).

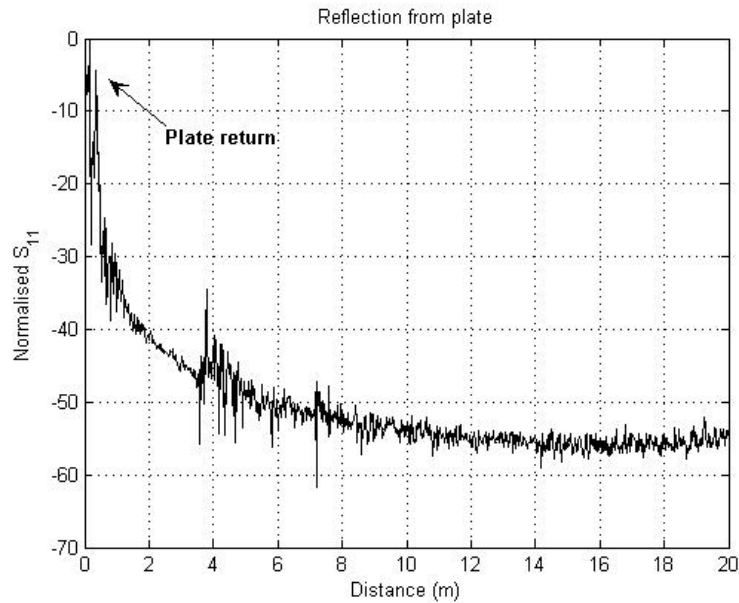


**Figure 5-14 Measured return from Aluminium plate**

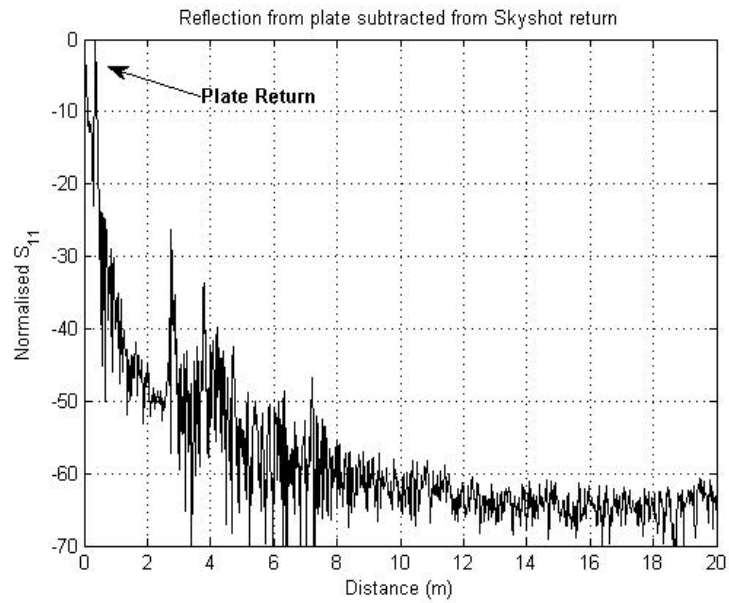


**Figure 5-15 Plate return after sky shot removal**

Next, the four-layer dielectric stack of figure 5-12 was set and measurements were taken. Figures 5-16 and 5-17 show the measured return before and after subtracting from the skyshot signal.

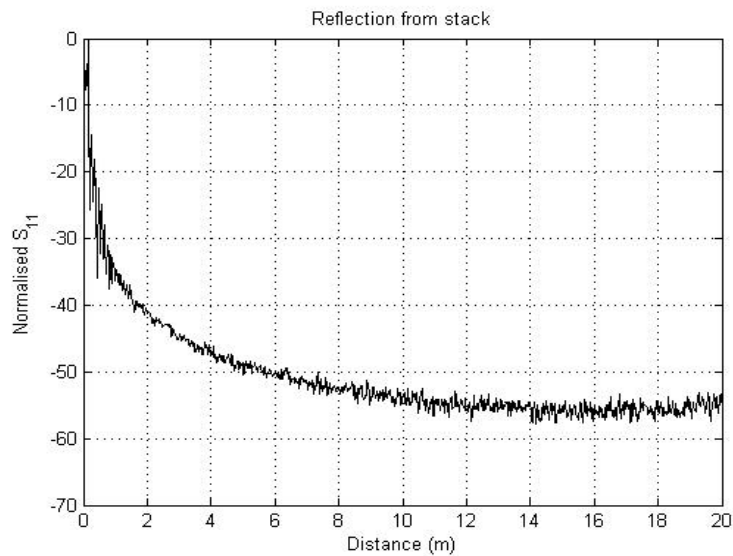


**Figure 5-16 Measured return from multilayered stack**

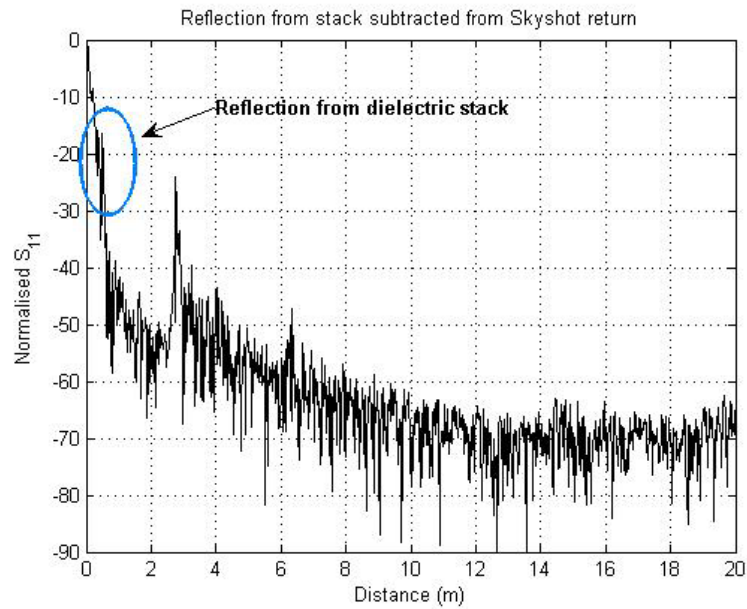


**Figure 5-17 Stack return after sky shot removal**

The residual mismatch between the antenna and the cable is removed by filtering and the filtered signal (in the linear scale) is shown in figure 5-18 below.

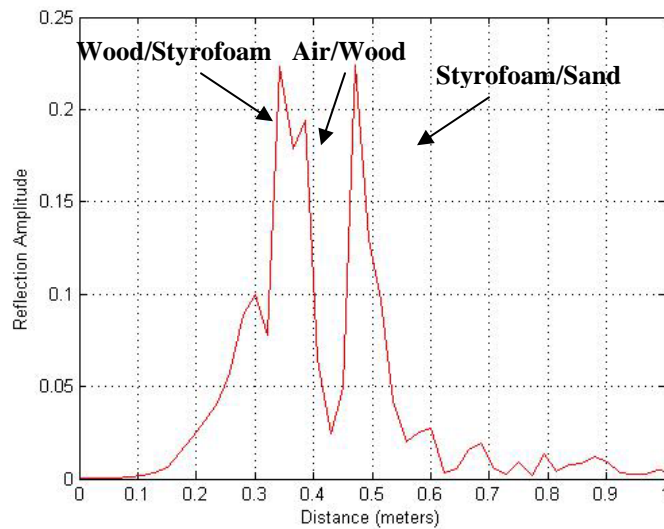


**Figure 5-18 Stack return after calibration and filtering**

Now, the MUSIC algorithm is applied on this signal to enhance the profile and estimate the time delays corresponding to signals. Figure 5-19 compares the range profiles obtained using FFT and MUSIC.

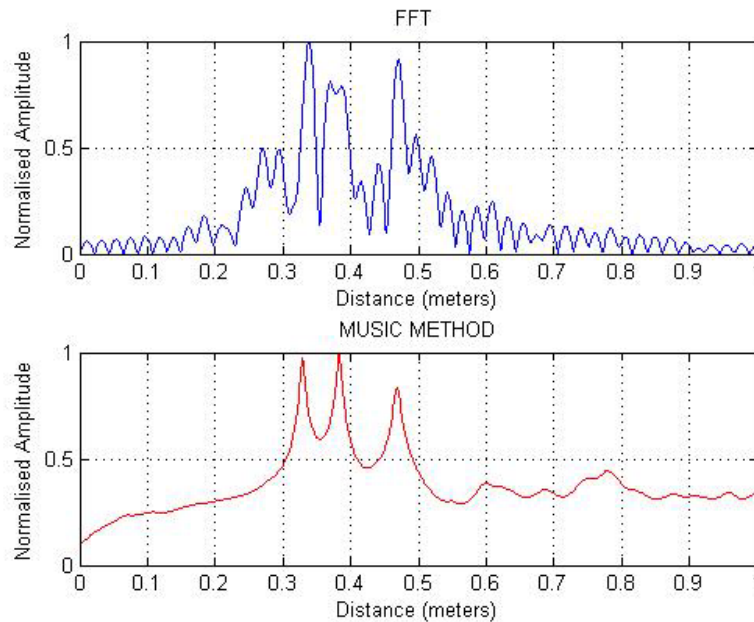


**Figure 5-19 Range Profiles obtained using FFT and MUSIC for multilayered stack**

Clearly, MUSIC is able to resolve the three major reflections as seen from figure 5-19. However, the Maximum Likelihood MUSIC estimator could not correctly estimate the reflection coefficients. This could be due to the non-Gaussian nature of noise. For estimating the amplitudes, the layer stripping approach was used. The time delays corresponding to valid reflections were obtained using MUSIC and the amplitudes were estimated using the recursive equations of chapter 2. Figure 5-20 shows the reconstructed profile.

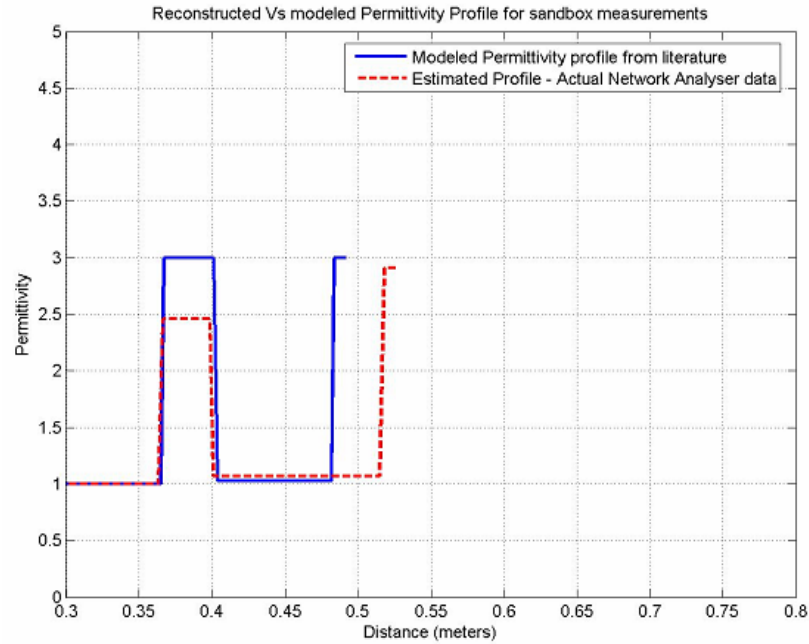


**Figure 5-20 Reconstructed Vs actual Permittivity profile of multilayered stack**

The reconstructed profile reasonably matches with the true profile. For the second layer, the algorithm has predicted a value of 2.5. However, the true value of permittivity of sand was not measured and since a value between 2.5 and 3.5 has been documented [29], a value of 3 was chosen for modeling. Hence, the algorithm has yielded a reasonable estimate. We also observe a deviation in the position of the third interface (between styrofoam and sand). This deviation can be attributed to the fact that a permittivity of 2 was chosen for velocity correction in order to identify the reflecting boundaries.

### 5.3 Experiments in Greenland

The Greenland sea-ice research team of the RSL used a prototype of a Plane Wave radar in Greenland during the summer 2004 season, with the objective of

estimating the thickness of snow over sea-ice. We used this data as yet another test case for the inversion algorithm. Table 5-6 shows the specifications of the radar prototype.

**Table 5-6 Network Analyzer Parameters for Plane Wave measurements in Greenland**

Type of radar	Step Frequency
Start Frequency	12 GHz
Bandwidth	6 GHz
Sweep Time	4.72 sec
No. of frequency points	801

Radar measurements were taken over a horizontal traverse of 80 m, with ten measurements every 1 meter. Core data was also collected at three different pits at the test site. Stratigraphy maps were observed at a couple of points along the grid. Figure 5-21 shows the relative positions of the core sampling areas with respect to the area where radar measurements were taken. It is clearly seen that Pit 2 is the only core reasonably close to any of the radar measurements and may provide a reasonable reference for radar measurement at the record marked 0. Hence, our objective was to invert the data at record 0 and compare the estimated permittivity profile with the core data and the stratigraphy map at record 0. Figure 5-22 shows the set-up of the plane wave experiment.

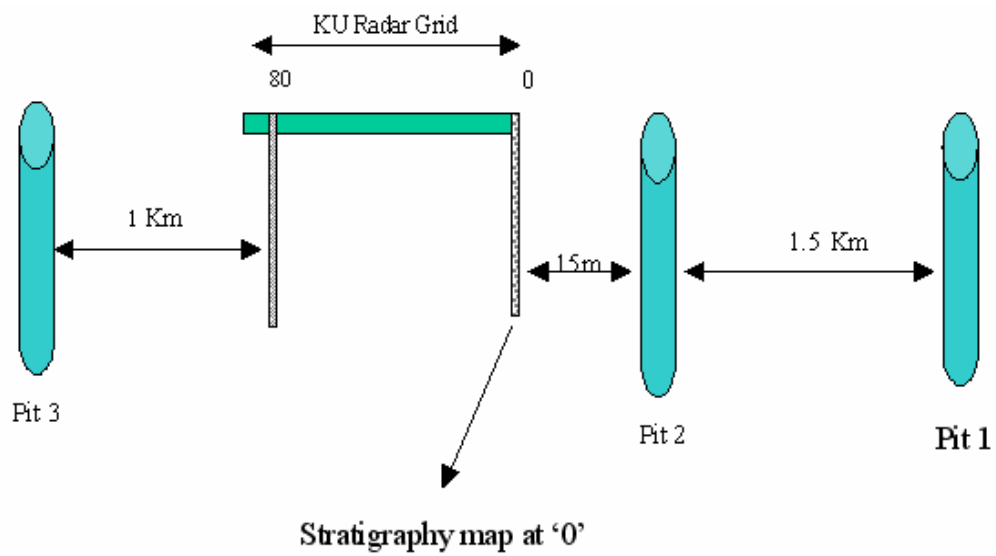


**Figure 5-21** Relative locations of measurement grid and cores

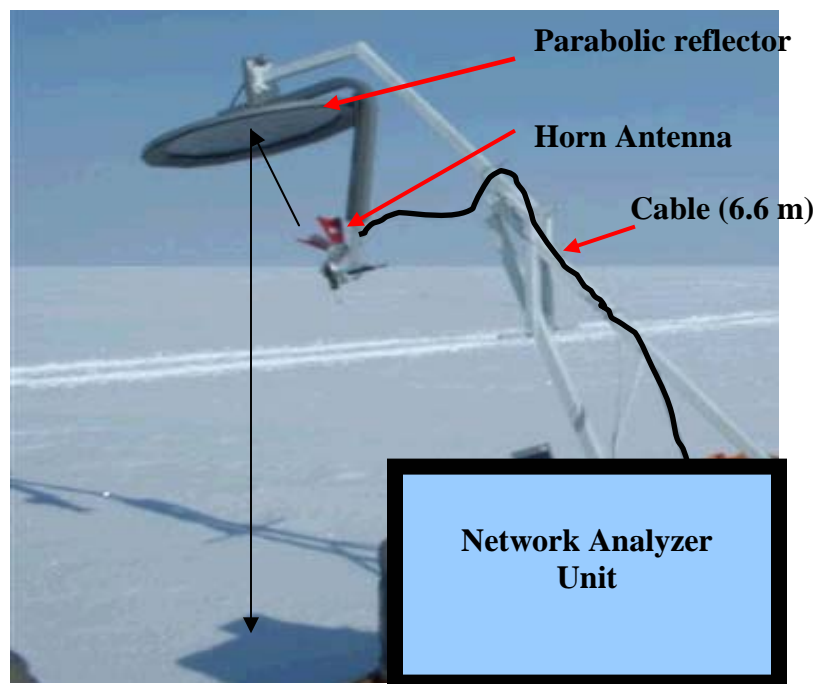


**Figure 5-22** Experimental set up of the plane wave test

The network analyzer is connected to a horn antenna which then radiates the transmitted signal to the parabolic reflector. The EM wave radiated from the reflector is approximately a plane wave. The network analyzer is calibrated at its terminals and hence the observed distances are with respect to this terminal. The cable connecting the horn antenna to the analyzer measured around 6.6 meters and “loop” distance between the horn and the snow surface is around 3.1 meters.

Figure 5-23 shows the echogram of the measurements along the grid. It can be seen that the surface layer (marked as 1) occurs around a distance of 9.7 meters (6.6 meters of the cable plus a loop of 3.1 meters) followed by two discontinuous layers (marked as 2) at around 10.5 meters, 10.7 meters. The echogram also shows indicates the presence of a discontinuous layer at around 11.6 meters (marked as 3). Layers 2 and 3 could be annual snow layers which get compressed leading to higher densities.

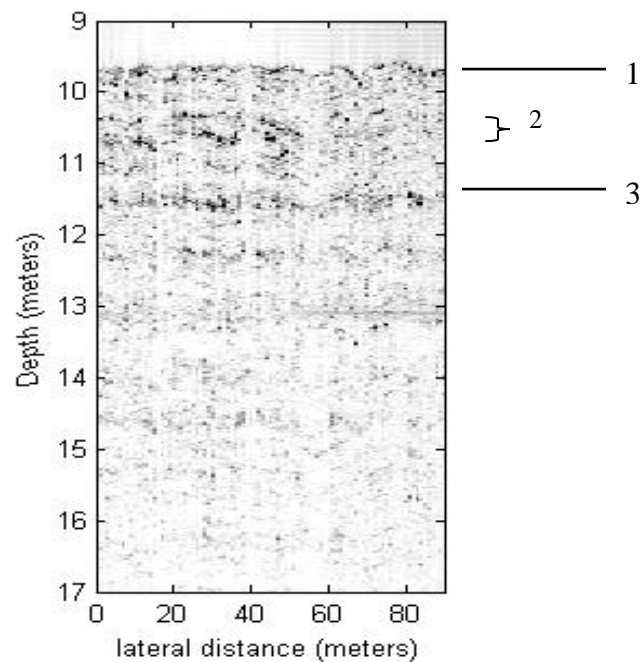
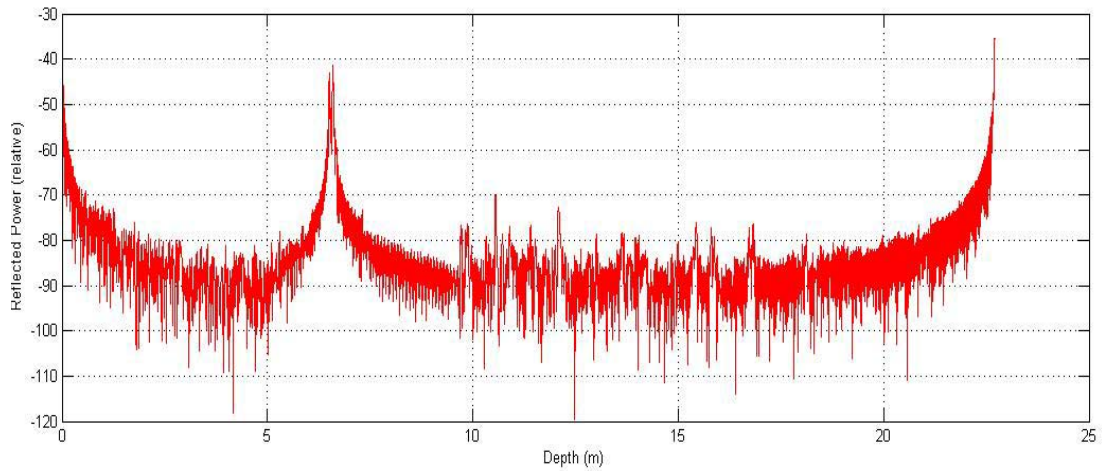
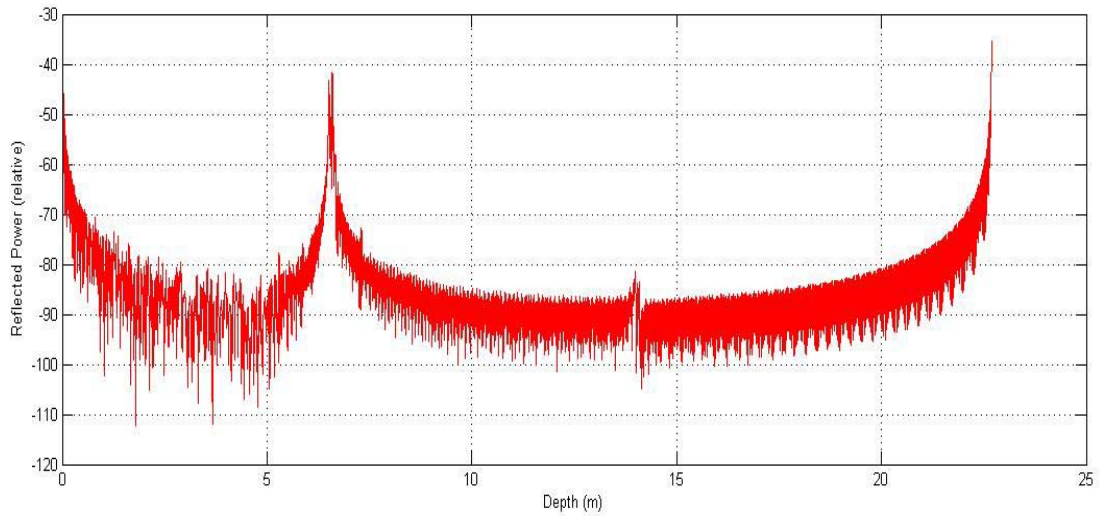


Figure 5-23 Echogram of radar measurements along the KU radar grid

Figure 5-24 shows the radar measurements at record 0. The reflection occurring at 0 meters is due to the impedance mismatch between the network analyzer terminal and the cable. This is removed by taking measurements by tilting the horn antenna skyward (figure 5-25) and subtracting it from the actual signal (from snow) as shown in figure 5-26.



**Figure 5-24 Radar measurement at record 0 (including the impedance mismatch at the origin)**



**Figure 5-25 Sky shot measurements**

The peak at around 6.5 meters is due to the mismatch between the cable and the horn antenna. The surface return is observed at around 9.7 meters.

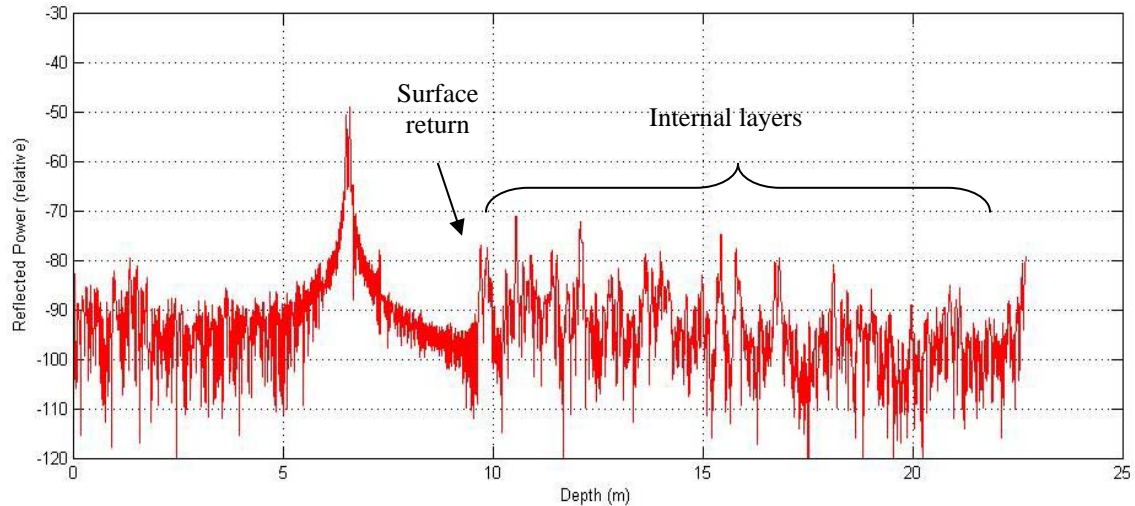


**Figure 5-26 Radar measurement at record 0 (after subtracting the sky shot return)**

Here, an interesting observation in the above figure is that several reflections corresponding to internal layers are higher than the surface return. Intuitively, it can be understood that inverting this profile directly would lead to abnormal values of permittivity (because of abnormal reflection amplitudes) and hence the observed data needs to be analyzed and any irregularities need to be removed.

These strong peaks could be due to several reasons- abrupt density changes, multiple reflections from internal snow layers, clutter due to scattering effects, system noise or due to reflections from static objects like the antenna pole. Since the inversion algorithm works best on data free from system effects and clutter, it is necessary to eliminate these effects before applying the inversion algorithm on this data.

A good way to check for reflections from stationary targets is to compare adjacent records and look for similarity in the occurrences of peaks at the locations of interest. Applying the same test to our problem, we found no consistency in the appearance of the stronger reflections. Hence, we can conclude that these reflections are not from stationary targets.

From the density data of the nearest core (Pit 2), the permittivity profile at the site was modeled using the dry snow permittivity model [9]. Figure 5-27 shows the modeled permittivity profile from the snow surface upto a depth of 11.92 meters which is equivalently 200 centimeters into the snow subsurface.

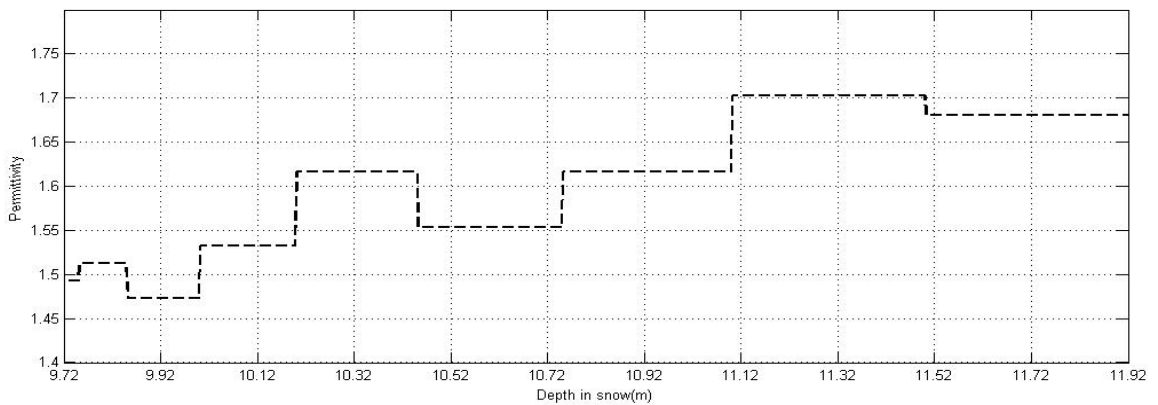


**Figure 5-27 Permittivity profile of Pit 2 modeled using the dry snow model**

The maximum value of permittivity is found to be 1.7. It can be inferred that there is no drastic change in permittivity that could cause spikes to appear in the range profile. Using this profile, the range profile was modeled using ADS so that the effect of multiple reflections can be analyzed. Figure 5-28 shows a plot of the

modeled range profile. This figure is compared with a profile of the observed return at record 0 (Figure 5-29).

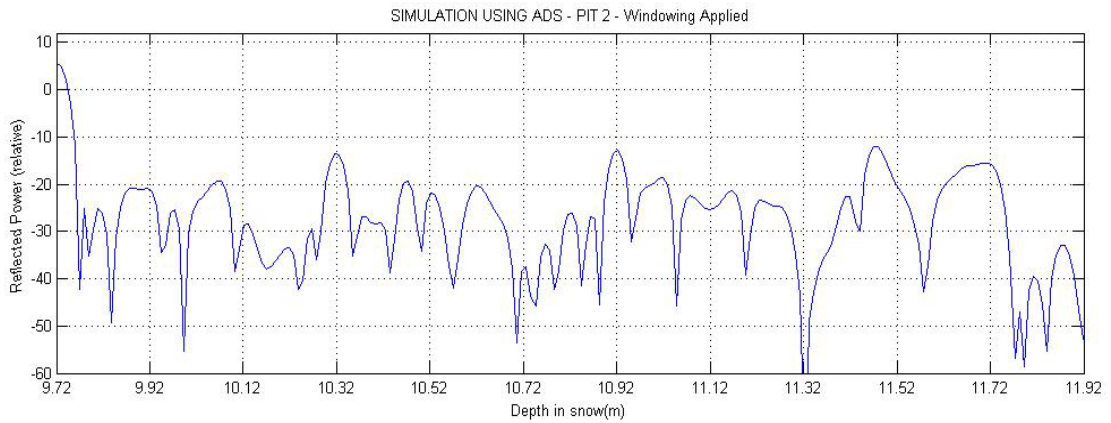


**Figure 5-28 Simulated radar return of Pit 2 using ADS**

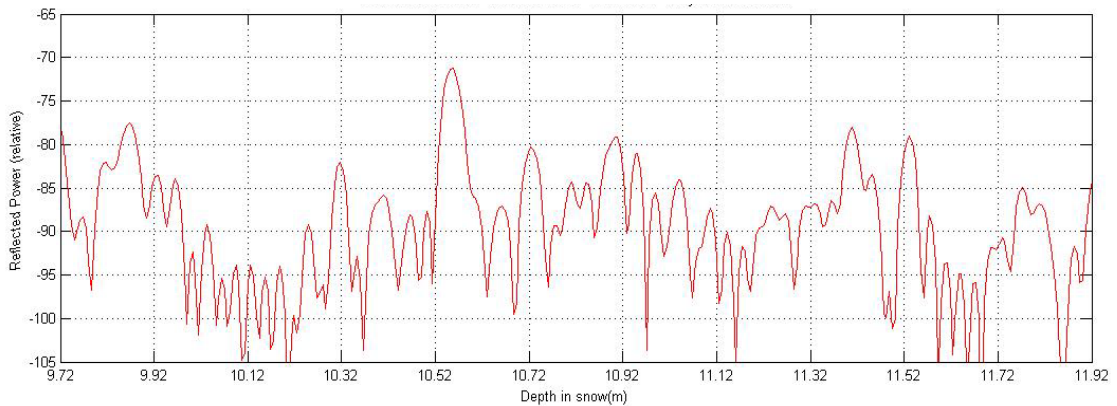


**Figure 5-29 Actual radar return at record 0**

We find that there are several inconsistencies in the above comparison. Clearly, the ADS simulation shows that the surface return is dominant whereas the actual data shows the presence of several strong returns either comparable to or greater than the surface return. Also, the positions of many of the peaks do not match well. Hence, we have insufficient information for this problem. However, the

inversion algorithm was applied on this data (after calibration) and as expected, the algorithm yielded unusual values of permittivity for the internal snow layers, which is contradictory to the permittivity values indicated by the core measurements.

Therefore, it was decided to test the inversion algorithm on data simulated using ADS. Figure 5-30 compares the range profiles obtained using FFT and MUSIC. Clearly, MUSIC is able to resolve internal reflections which appear embedded with the sidelobes of stronger returns. From this enhanced profile, delays corresponding to signal peaks were chosen and fed into the estimator and the estimated permittivity profile is plotted in figure 5-31.

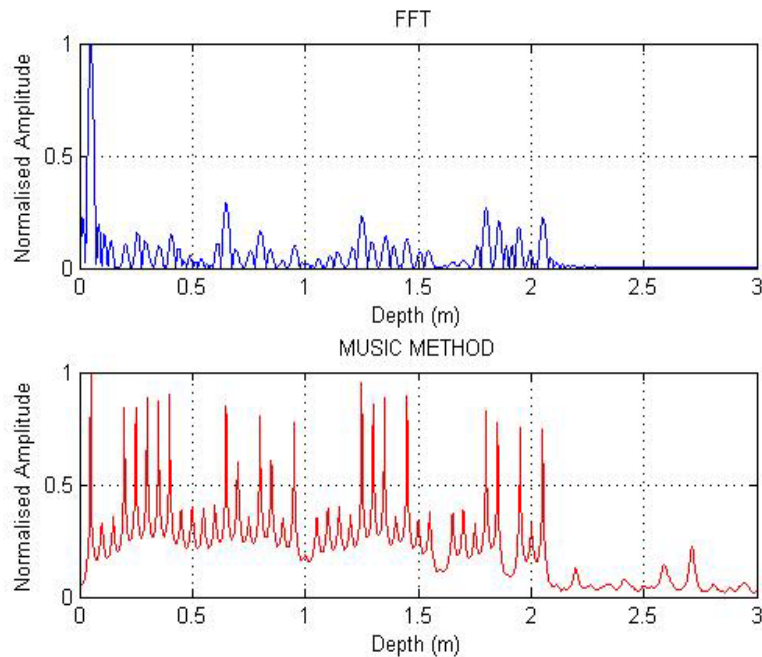


**Figure 5-30 Range Profiles of simulated data obtained using FFT and MUSIC**

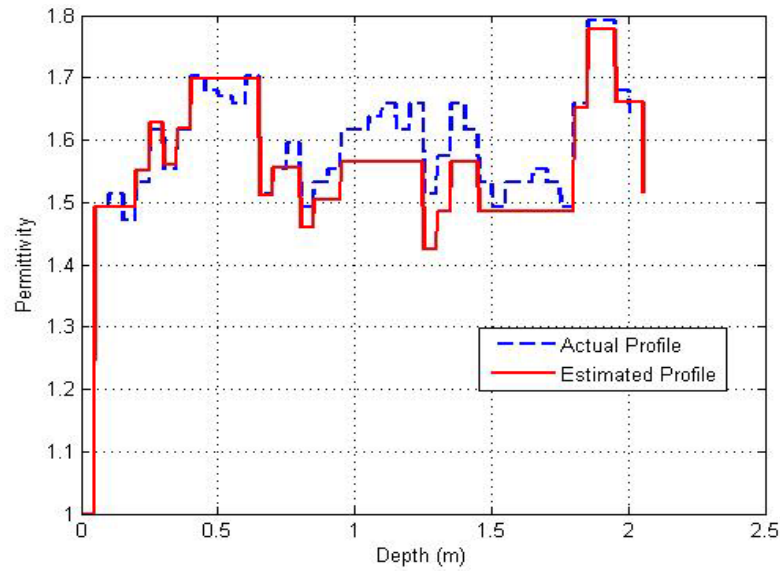


**Figure 5-31 Reconstructed permittivity profile Vs actual (modeled) profile**

## Summary

In this chapter, the inversion algorithm was tested on data collected using a radar system. It was found that the MUSIC algorithm performed really well on the FMCW radar data from Antarctica, but was only partly successful when tested on the sandbox experiment. However, in conjunction with the layer stripping method, we were able to successfully invert the data. The test on Plane wave data is still under research and with sufficient information about the internal layers of snow, the data can be inverted. In conclusion, we find that the performance of the inversion algorithms depends on several factors such as the quality of the measurement, the accuracy of the model used for inversion and the contribution of external factors (which cannot be modeled or accounted for).

## Chapter 6

# GUI for the Inversion Algorithm

---

In order to make the inversion algorithm user-friendly and easy to use, a Graphical User Interface (GUI) in MATLAB was developed. Figure 6-1 shows a snapshot of the GUI.

There are essentially four important modules in this GUI :

### **1. Parameter declaration and File Selection:**

Here, the user enters basic radar parameters such as type of radar, start frequency, bandwidth, sweep time and also selects the recorded radar data file. Two of the commonly used radars in geological exploration are the Frequency Modulated Continuous Wave (FMCW) radar and the Stepped-Frequency radar. Though the procedure for inversion is same for both these radars, they follow different mathematical models. In this GUI, the model will be chosen based on the user's choice. The data file needs to be stored in the local computer and should be chosen by the user. A couple of recorded radar data files taken by the RSL (which were successfully inverted using this GUI) can also be chosen by the user to get a better understanding of the working of the algorithm. The user can view an A-scope of the chosen data file. Also, the echogram of the total measurement can be plotted.

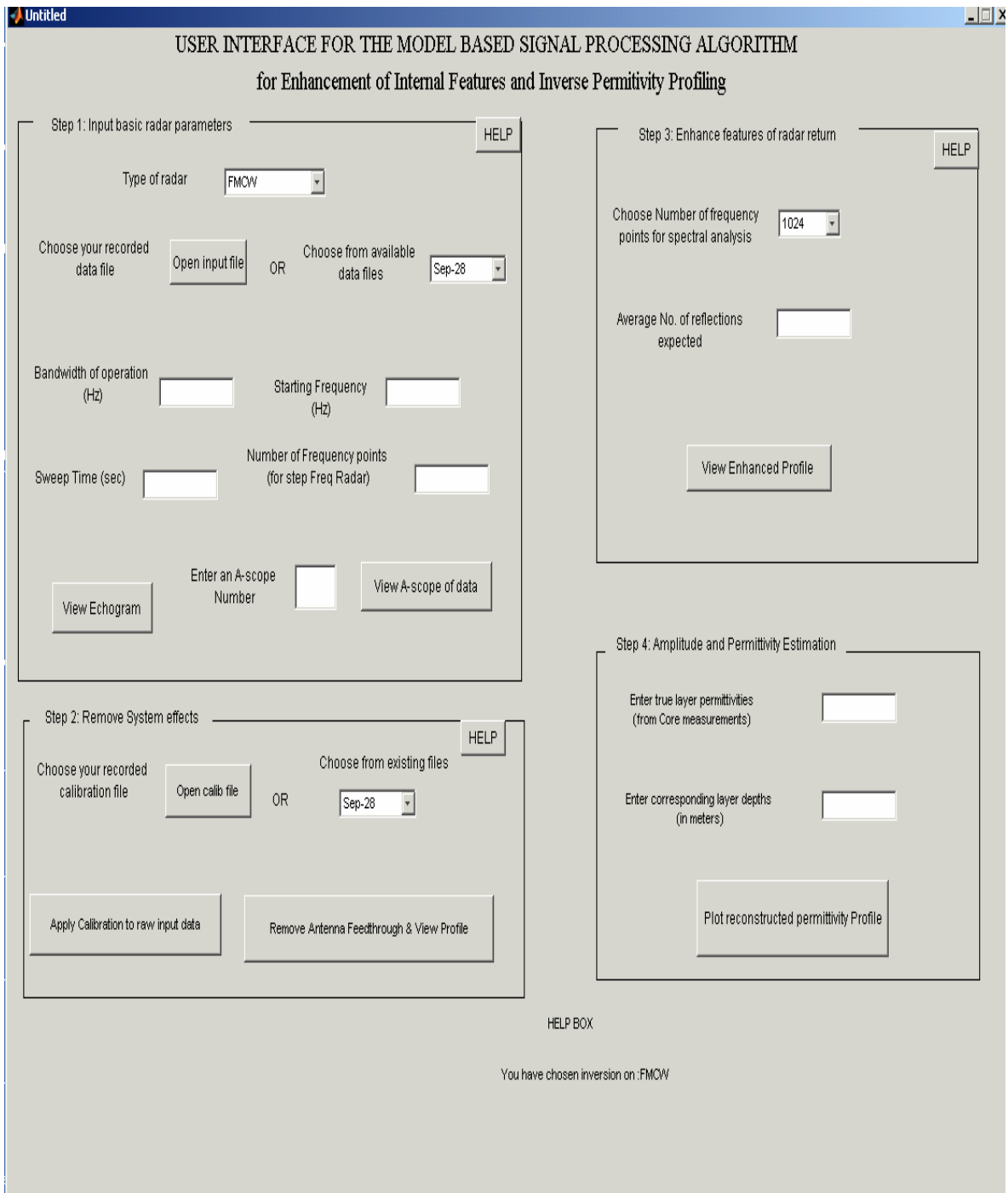


**Figure 6-1 Snapshot of the GUI for Data Inversion**

## **2. System effect removal:**

In order to obtain the target impulse response (or transfer function), the effects of the system need to be removed. As discussed in chapter 5, this is usually done by deconvolution of the total radar response with the system transfer function. The transfer function of the whole radar system can be measured by taking measurements on a flat metal plate (also called calibration). Hence, to begin processing the data, the user has to load the calibration data file. If the user has selected an RSL data file, then the corresponding calibration should be chosen. The next step in the inversion process is to remove the antenna feed through (if the radar system is operating in bistatic mode) by filtering. The filter module is invoked when the user selects the appropriate button in the GUI.

## **3. Enhancement of features:**

To apply MUSIC algorithm on the data, the user needs to feed in parameters such as the number of frequency samples and a guess on the number of reflections (sinusoids) that will be expected in the estimation process. For example, if the data has been taken from an environment where the density distribution is expected to be fairly inconsistent, it is advisable to choose the number of reflections to be somewhere between 20-30. However, in a scenario where homogeneous dielectric layers are expected to dominate (water, sand), we may choose values than 10. Hence, some apriori information will help to yield a smoother permittivity profile. Once

these parameters are fed in, the GUI invokes the MUSIC algorithm and plots the high-resolution frequency spectrum of the data.

#### **4. Permittivity Estimation:**

From the frequency spectrum, the user sets a threshold looking at the amplitude of the peaks of the enhanced profile. MUSIC then estimates the reflection coefficients corresponding to the beat frequencies and converts them into time delays and then estimates the unknown permittivities. Finally, it plots the estimated permittivity values with depth.

# Chapter 7

## Summary and Future Work

---

### 7.1 Summary

Ground penetrating radars are being used to characterize features of the surface and the sub-surface. However, the GPR data are corrupted with noise, scattering, and losses due to the random nature of the underlying subsurface. To this end, a model based algorithm was implemented and tested for the purpose of estimating the permittivity profile.

Algorithms based on MMSE minimization (Gauss-Newton) and spectral estimation (MUSIC) were developed (chapter 3) and first tested on synthetic data cases in chapter 4. It was found that the MUSIC algorithm – a spectral estimation technique was more robust and is suitable for tests on actual radar data.

In chapter 5, the MUSIC algorithm was applied on radar data collected during field experiments in Antarctica using an FMCW radar and on tests conducted at the sandbox facility at the RSL lab using a network analyzer. It was found that the MUSIC algorithm performed reasonably well in inverting data collected using the FMCW radar. There were a few errors in the estimation and the possible causes for the deviation were also discussed. In the sandbox test, MUSIC was only partly successful; however, in conjunction with the layer stripping method, we were able to

successfully invert the data. Finally, a Graphical user interface for the model based inversion algorithm was also developed in MATLAB.

## **7.2 Future Work**

The accuracy of model based techniques for data inversion depends on several factors, here are a few:

1. Accuracy of the mathematical model that represents the radar response
2. Accuracy of the measurement and calibration system
3. Signal to noise ratio of the system
4. Effects of clutter and scattering due to rough surface

Hence it is important that the mathematical model be thoroughly tested using several cases of synthetic data. Calibration errors can drastically change the amplitude and phase of the actual signal and hence, the calibration system should be robust.

In this work, we have only considered the case of specular reflection and the effects of clutter, surface scattering and attenuation have been neglected from the model. Incorporating these effects into the model can enhance the performance of the inversion algorithm.

Inversion methods based on three dimensional modeling such as the Method of Moments (MOM) and Finite Difference Time Domain (FDTD) take into account the effects of scattering due to random surfaces and the three dimensional antenna beam pattern and hence they can be implemented for the forward model to yield better inversion results.

## References:

- [1] Mars Instrument Development Project (MIDP) Technical document, JPL, NASA, 2002.
- [2] L.P.Peters,Jr., J. J. Daniels, and J. D. Young, “Ground penetrating radar as a subsurface environmental sensing tool,” *Proceedings of the IEEE*, vol. 82, pp. 1802–1822,Dec. 1994.
- [3] G. Picardi et al., “The Mars Advanced Radar for Subsurface and Ionosphere Sounding (MARSIS): concept and performance,” *Proceedings of the IEEE International Geoscience and Remote Sensing Symposium*, Hamburg, Germany, pp. 2674-2677, 1999.
- [4] Carl Leuschen, “Surface Penetrating Radar for Mars Exploration,” *PhD Dissertation*, Electrical Engineering and Computer Science, The University of Kansas, 2001.
- [5] R. Togneri , “Estimation Theory for Engineers”, Dept. of Electrical, Electronic and Computer Engineering, The University of Western Australia, 2001 [online] Available: [http://www.ee.uwa.edu.au/~roberto/teach/Estimation\\_Theory.pdf](http://www.ee.uwa.edu.au/~roberto/teach/Estimation_Theory.pdf)
- [6] Albert Tarantola, *Inverse Problem Theory*, Elsevier Press, New York, 1987.
- [7] D.J.Daniels, “Ground Penetrating Radar - second edition”, Chapter – 11, IEE Radar, Sonar, Navigation and Avionics Series 15, 2004
- [8] G.S. Brown, “The Average Impulse Response of a Rough Surface and its Applications”, *IEEE Transactions on Antennas and Propagation*, vol.25, pp. 67- 74, 1977.

- [9] F.T. Ulaby, R.K. Moore, and A.K. Fung, *Microwave Remote Sensing Active and Passive: Vol.3 – From Theory to Applications*: Artech House, 1982.
- [10] F.T. Ulaby, R.K. Moore, and A.K. Fung, *Microwave Remote Sensing Active and Passive: Vol. 2 Radar Remote Sensing and Surface Scattering and Emission Theory*: Artech House, 1982.
- [11] Carl Leuschen, et.al, “Simulation and design of Ground-Penetrating radar for Mars Exploration”, *Proceedings of the 2001 International Geoscience and Remote Sensing Symposium IGARSS '01*, Sydney, Australia, July 2001.
- [12] Vijay Ramasami, *A Simulation Package for Radar Systems*, Radar and Remote Sensing Laboratory, Information and Telecommunication technology Research Center, The University of Kansas, 2003
- [13] Olaf Eisen, “On the nature, interpretation, and application of electromagnetic reactions in cold ice”, *PhD Dissertation*, Electrical Engineering, The Alfred Wegener Institute for Polar and Marine Research, Germany, 2002.
- [14] Steven M.Kay, *Fundamentals of Statistical Signal Processing : Vol I – Estimation Theory*, Prentice Hall, New Jersey, 1993
- [15] G.A.F. Seber, C.J.Wild, *Nonlinear Regression*, J.Wiley, New York, 1989
- [16] Umberto Spagnolini, “Permittivity Measurements of Multilayered Media with Monostatic Pulse radar,” *IEEE Transactions on Geoscience and Remote Sensing*, Vol. 35, No.2, pp. 454–463, March 1997.

- [17] S. Stergiopoulos, editor, "Advanced Signal Processing handbook: Theory and implementation for radar, sonar & medical imaging Real-time systems", Chapter 5, RC Press, 2000
- [18] "Nonlinear Least Squares Regression", [online] Available at:  
<http://www.itl.nist.gov/div898/handbook/pmd/section1/pmd142.htm>
- [19] Available at: [http://www.curvefit.com/local\\_minimum.htm](http://www.curvefit.com/local_minimum.htm)
- [20] Ronald Gallant, *Nonlinear Statistical Models* : John Wiley & Sons, 1993
- [21] Monson Hayes, *Statistical Digital Signal Processing and Modeling*, J.Wiley,1996
- [22] R.Schmidt, "Multiple emitter location and signal parameter estimation", *Proceedings of RADC Spectrum Estimation Workshop*, pp 243-258, 1979
- [23] H.Yamada, et.al., "Super resolution techniques for time-domain measurements with a network analyzer ," *IEEE Transactions on Antennas and Propagation*, Vol. 39, No.2, February 91, pp. 454-462.
- [24] Kuok Wai Wong, "Development of a Prototype of a 2-8 GHz FMCW Radar for Snow Thickness Measurement on Sea Ice", Master's Thesis, , Electrical Engineering and Computer Science, The University of Kansas, 2004.
- [25] Sudarsan Krishnan, "Modeling and Simulation Analysis of a FMCW Radar for Measuring snow Thickness," Master's Thesis, , Electrical Engineering and Computer Science, The University of Kansas, 2004.

- [26] A.Stogryn, "Equations for calculating the dielectric constant of saline water," IEEE Transactions on Microwave Theory Tech., vol. MTT-19, pp. 733–736, 971.
- [27] D.G.Barber,et al ., "Statistical characterization of the geo-physical and electrical properties of snow on landfast first-year sea ice," Journal of Geophysical Research, Vol. 100, No.C2, Feb 95, pp. 2673-2686.
- [28] John Paden,"Bistatic/Monostatic Synthetic Aperture Radar for Ice Sheet Measurements ," Master's Thesis, Electrical Engineering and Computer Science, The University of Kansas, 2003.
- [29] Available at:  
<http://zhangzc.jahee.com/chemcai/Dielectric%20Constant%20Table.htm#SECTION-S>
- [30] F.T. Ulaby, R.K. Moore, and A.K. Fung, *Microwave Remote Sensing Active and Passive*: Vol. 1, Norwood, MA: Artech House, 1982.
- [31] Available at:  
<http://www.s2.chalmers.se/~viberg/MBSP/lect7.pdf>